Neurobiology of Disease 132 (2019) 104589

Contents lists available at ScienceDirect

Neurobiology of Disease

journal homepage: www.elsevier.com/locate/ynbdi

Altered microglia and neurovasculature in the Alzheimer's disease cerebellum

Malvindar K. Singh-Bains[a,b], Vanessa Linke[a,b], Micah D.R. Austria[a,b], Adelie Y.S. Tan[a,b], Emma L. Scotter[a,c], Nasim F. Mehrabi[a,c], Richard L.M. Faull[a,b], Mike Dragunow[a,c,*]

[a] Centre for Brain Research, University of Auckland, Private Bag 92019, Auckland 1142, New Zealand
[b] Department of Anatomy and Medical Imaging, University of Auckland, Private Bag 92019, Auckland 1142, New Zealand
[c] Department of Pharmacology and Clinical Pharmacology, University of Auckland, Private Bag 92019, Auckland 1142, New Zealand

ARTICLE INFO

Keywords:
Alzheimer's disease
Neocerebellum
Cerebellum
Human brain
Tissue microarrays

ABSTRACT

Traditionally regarded to coordinate movement, the cerebellum also exerts non-motor functions including the regulation of cognitive and behavioral processing, suggesting a potential role in neurodegenerative conditions affecting cognition, such as Alzheimer's disease (AD). This study aims to investigate neuropathology and AD-related molecular changes within the neocerebellum using post-mortem human brain tissue microarrays (TMAs).

Immunohistochemistry was conducted on neocerebellar paraffin-embedded TMAs from 24 AD and 24 matched control cases, and free-floating neocerebellar sections from 6 AD and 6 controls. Immunoreactivity was compared between control and AD groups for neuropathological hallmarks (amyloid-β, tau, ubiquitin), Purkinje cells (calbindin), microglia (IBA1, HLA-DR), astrocytes (GFAP) basement-membrane associated molecules (fibronectin, collagen IV), endothelial cells (CD31/PECAM-1) and mural cells (PDGFRβ, αSMA).

Amyloid-β expression (total immunolabel intensity) and load (area of immunolabel) was increased by > 4-fold within the AD cerebellum. Purkinje cell counts, ubiquitin and tau immunoreactivity were unchanged in AD. IBA1 expression and load was increased by 91% and 69%, respectively, in AD, with no change in IBA1-positive cell number. IBA1-positive cell process length and branching was reduced by 22% and 41%, respectively, in AD. HLA-DR and GFAP immunoreactivity was unchanged in AD. HLA-DR-positive cell process length and branching was reduced by 33% and 49%, respectively, in AD. Fibronectin expression was increased by 27% in AD. Collagen IV, PDGFRβ and αSMA immunoreactivity was unchanged in AD. The number of CD31-positive vessels was increased by 98% in AD, suggesting the increase in CD31 expression and load in AD is due to greater vessel number. The PDGFRβ/CD31 load ratio was reduced by 59% in AD.

These findings provide evidence of molecular changes affecting microglia and the neurovasculature within the AD neocerebellum. These changes, occurring without overt neuropathology, support the hypothesis of microglial and neurovascular dysfunction as drivers of AD, which has implications on the neocerebellar contribution to AD symptomatology and pathophysiology.

1. Background

Alzheimer's disease (AD), a chronic neurodegenerative condition, is the most common form of dementia and involves the progressive degradation of cognitive and social-emotional function. The two main neuropathological hallmarks of AD are the intracellular aggregation of hyperphosphorylated tau into neurofibrillary tangles and the extracellular accumulation of amyloid-β peptide which forms amyloid plaques (Braak and Braak, 1991; Braak and Braak, 1997a; Braak and Braak, 1997b; Thal et al., 2002). The majority of AD research has focused predominantly on disease-associated changes in the cerebral cortex. However, the role of the cerebellum in AD has received little

Abbreviations: α-SMA, Alpha-smooth muscle actin; AD, Alzheimer's disease; ARP score, Age-related plaque score; BBB, Blood-brain barrier; CB, Cerebellum; CCAS, Cerebellar cognitive affective syndrome; CD31, Cluster of differentiation 31; CERAD, Consortium to Establish a Registry for Alzheimer's Disease; DAB, 3,3′-diaminobenzidine; ECM, Extracellular matrix; GFAP, Glial fibrillary acidic protein; H_2O_2, Hydrogen peroxide; HLA-DR, Human leukocyte antigen D-related; MHCII, Major histocompatibility complex class II; milliQ H_2O or mQ H_2O, Milli-Q water; PBS, Phosphate-buffered saline; PBS-T, Phosphate-buffered saline with Triton X-100; PDGFRβ, Platelet-derived growth factor receptor-beta; PECAM-1, Platelet endothelial cell adhesion molecule – 1; ROI, Region of interest; TMA, Tissue microarrays

* Corresponding author at: Centre for Brain Research, The University of Auckland, Private Bag 92019, Auckland 1142, New Zealand.
E-mail address: m.dragunow@auckland.ac.nz (M. Dragunow).

https://doi.org/10.1016/j.nbd.2019.104589
Received 29 April 2019; Received in revised form 30 July 2019; Accepted 23 August 2019
Available online 24 August 2019
0969-9961/

attention, often serving as control tissue or a reference region in AD studies (Smith et al., 1997; Dukart et al., 2010).

Traditionally, the cerebellum was widely regarded as a structure controlling motor regulation such as movement, gait, posture, motor coordination and learning (Albus, 1971; Thach, 1996; Wegiel et al., 1999). However, recent clinical and neuroimaging studies have demonstrated that the cerebellum exerts non-motor functions such as cognitive, behavioral and affective processing (Schmahmann and Sherman, 1998; Schmahmann et al., 2001; Baumann et al., 2015). In addition, the description of cerebellar cognitive affective syndrome (CCAS), a condition characterized by the presence of cerebellar lesions, includes hallmark deficits in executive function, linguistic processing, visuospatial cognition and emotional modulation. This clinical evidence supports the hypothesis that changes in the cerebellum lead to compromised cognitive and affective functions, rather than just motor symptoms (Schmahmann and Sherman, 1998; Schmahmann, 2004).

Pathological changes within the cerebellum have been reported in AD by early descriptive and semi-quantitative studies in human tissue. Cerebellar amyloid-β deposits have been frequently reported within the molecular, granular and Purkinje cell layers of the cerebellar cortex (Braak et al., 1989; Joachim et al., 1989; Dickson et al., 1990; Li et al., 1994; Fukutani et al., 1997; Wegiel et al., 1999; Wang et al., 2002). In contrast, neurofibrillary tau tangles are largely absent (Joachim et al., 1989; Li et al., 1994; Wegiel et al., 1999; Yamamoto and Hirano, 1985). Semi-quantitative studies have reported a loss of Purkinje cells within the AD cerebellum compared to control brains (Sjöbeck and Englund, 2001; Wegiel et al., 1999). However, a recent stereological cell counting study reported no overall loss of Purkinje cells, suggesting that neuronal cell bodies are widely intact in the AD cerebellum (Andersen et al., 2012). Since this study, the literature concerning AD cerebellar neuropathology has been limited to predominantly historical observations.

Interestingly, the importance of the cerebellum in neurodegenerative conditions such as frontotemporal dementia and AD has recently been gaining traction in patient neuroimaging and proteomics studies (Bas et al., 2009; Canu et al., 2010; Guo et al., 2016; Xu et al., 2018). Recent functional neuroimaging studies in humans and previous tracing studies in animal brains have documented the extensive, topographically-organized connections between the cerebral cortex and cerebellum (Haines et al., 1997; Haines and Dietrichs, 1984; Siwek and Pandya, 1991; Habas et al., 2009; Buckner et al., 2011). Notably Guo et al. (2016) reported that cerebellar regions with greater atrophy (cerebellar crus I and II) are those connected via cerebral 'default modes' to regions of the cerebral cortex (bilateral angular gyrus, precuneus and posterior cingulate cortex) which are more vulnerable to AD degeneration (Guo et al., 2016). Together, these findings of alterations in the cerebellum in recent neuroimaging studies suggest that the cerebellum is not a "silent bystander" or a mere "reference point" for neuroanatomical studies of AD (Guo et al., 2016; Schmahmann, 2016). A recent proteomics study mapped the relative levels of over 5000 distinct proteins within $n = 9$ AD and n = 9 control human cases from the Neurological Foundation of New Zealand Human Brain Bank (Xu et al., 2018). Unexpectedly, 120 proteins demonstrated cerebellar-specific changes which included proteins involved in dysregulation of the mitochondrial electron transport chain. Therefore, in light of recent clinical neuroimaging studies supporting network-selective vulnerability of the cerebellum to AD, the recognition of the cerebellum in non-motor circuits relating to cognition, combined with the identification of cerebellar-specific protein changes in AD using proteomics, suggest that there would be great merit in conducting a robust examination into the AD-related molecular changes within the human cerebellum at the cellular level.

The aim of this study is to utilize a tissue microarray (TMA) screening approach to examine molecular changes in the human AD neocerebellum, with a focus on neuropathological hallmarks, Purkinje cells, and non-neuronal cells involved in neuroinflammation and cerebrovascular dysfunction including microglia, endothelial cells, perivascular cells, and basement membrane-associated molecules. We hypothesize that the human cerebellum will present with changes in non-neuronal cells including microglia and vascular cells, based on the accumulation of literature suggesting that neuroinflammation and cerebrovascular dysfunction may precede the onset of neurodegenerative changes in AD and animal models (Bell and Zlokovic, 2009; Lepelletier et al., 2017; Heppner et al., 2015). Because historical neuropathological studies have found a lesser degree of AD pathology in the cerebellum compared to cortical regions, the identification in the cerebellum of more subtle AD-related molecular changes which would be difficult to detect in more severely degenerated regions, provides the possibility of detecting early drivers of AD pathogenesis.

2. Materials and methods

2.1. Human tissue collection and processing

All post-mortem human brain tissue used in this study was obtained from the Neurological Foundation of New Zealand Human Brain Bank in the Centre for Brain Research, University of Auckland. All protocols in this study were approved by the University of Auckland Human Participants Ethics Committee (2008/279 and 011654), and all families provided informed consent. All cases were examined by an independent neuropathologist and were classified based on neurological abnormalities, or lack thereof in neurologically normal control cases. To confirm a diagnosis of Alzheimer's disease (AD), the cases were pathologically classified according to the age-related plaque score (ARP) as outlined by the Consortium to Establish a Registry for Alzheimer's Disease (CERAD) for cases received prior to (2008) (Mirra et al., 1991). Cases received after (2008) were also classified according to Braak and Braak staging (I-VI) (Braak and Braak, 1991; Braak and Braak, 1995).

Fixation and dissection protocols for human brain tissue preparation have been described previously (Waldvogel et al., 2007; Waldvogel et al., 2008). Briefly, the brains were perfused and in each case the cerebellum was cut into four equal sized blocks from lateral to medial (CB0, CB1, CB2, and CB3) regions of the cerebellum, as shown in Fig. 1. For this study, the CB1 block of the neocerebellum from the right cerebellar hemisphere was used (Fig. 1). A small portion of the block (~3 mm thick section) was embedded in paraffin for paraffin immunohistochemistry and tissue microarray (TMA) production, while the bulk of the block was post-fixed by immersion, cryoprotected, frozen using powdered dry ice, and stored at −80 °C until preparation for free-floating immunohistochemistry.

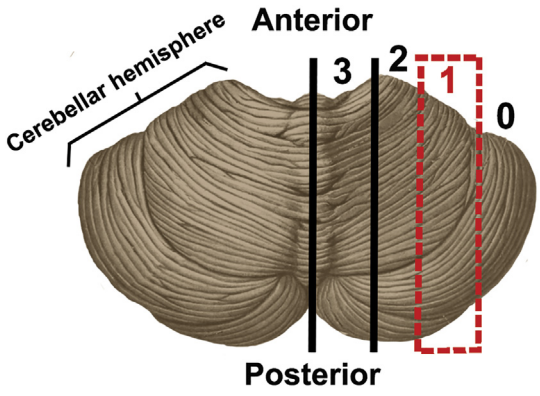

Fig. 1. Preparation of human cerebellum for tissue microarray and immunohistochemistry. In this study, the human cerebellum was dissected into four equal-sized blocks, from lateral to medial (blocks 0–3). Block 1 from the mid-region of neocerebellum was selected for this study. A small portion of the block (~3 mm thick section) was embedded in paraffin for paraffin immunohistochemistry and tissuemicroarray (TMA) production. The remainder of the block was post-fixed and prepared for free-floating immunohistochemistry.

Table 1
Neurologically normal control cases for cerebellum tissue microarray (TMA 15).

Case	Sex	Age at death (years)	Post-mortem delay (hours)	Cause of death
02F393	F	87	11	Ischaemic heart disease
4680	M	80	12	Ischaemic heart disease
6013	F	69	11.5	Aortic aneurysm
H121	F	64	5	Pulmonary embolism
H122	F	72	9	Emphysema
H123	M	78	7.5	Aortic aneurysm
H124	M	49	13	Ischaemic heart disease
H136	M	75	13	Aortic aneurysm
H137	F	77	12	Ischaemic heart disease
H139	M	73	5	Ischaemic heart disease
H144	M	76	18.5	Aortic aneurysm
H145	M	54	6.5	Ischaemic heart disease
H148	M	64	7	Ischaemic heart disease
H150	M	78	11	Myocardial infarction
H152	M	79	18	Congestive heart failure
H153	M	76	6	Ischaemic heart disease
H155	M	61	7	Ischaemic heart disease
H156	M	89	19	Ischaemic heart disease
H160	M	77	23	Ischaemic heart disease
H164	M	73	13	Ischaemic heart disease
H169	M	81	24	Asphyxia
H215	F	67	23.5	Ischaemic heart disease
H226	F	73	48	Mesothelioma
H239	M	64	15.5	Ischaemic heart disease
Mean	7F/17M	72.3	14.1	
Standard deviation		9.5	9.3	

F = female; M = male.

A total of 24 control cases with no history of neurological abnormalities (Table 1) and 24 AD cases with confirmed AD pathology and a clinical history of dementia (Table 2) were used for cerebellar paraffin TMA studies. The control and AD cases were matched as closely as possible for age at death and post-mortem delay. The control cases included 7 females and 17 males, aged 49–89 (mean = 72.3 ± 9.5 years), with a post-mortem delay of 5–48 h (mean = 14.1 ± 9.3 h). The AD cases included 14 females and 10 males, aged 51–87 (mean = 75.0 ± 8.8 years), with a post-mortem delay of 4–36 h (mean = 14.2 ± 7.8 h). To validate the TMA results, whole neocerebellar section analysis was conducted for 6 control cases (Table 3) and 6 AD cases (Table 4) using free-floating immunohistochemistry.

2.2. TMA design and production

Brain tissue donor blocks containing neocerebellum (block CB1) from n = 24 control and n = 24 AD cases (Tables 1 and 2) were fixed, dehydrated and processed for wax embedding as described previously (Waldvogel et al., 2007). Five 7 μm thick sections were cut from each donor block using a paraffin microtome (RM2235, Leica) and mounted onto positively charged slides (Grale HDS) for antigenicity and neuroanatomical localisation studies utilising standard paraffin immunohistochemistry and cresyl violet staining procedures. One section from each donor block was immunolabelled for glial fibrillary acidic protein (GFAP, mouse anti-human, Sigma [G3893], 1:5000), which was selected based on the ubiquitous presence of the protein in both control and AD tissue. All donor blocks immunolabelled successfully with GFAP, which indicated an absence of fixation irregularities which could affect paraffin immunohistochemistry. An additional 7 μm section from each case was labelled with cresyl violet for neuroanatomical identification of a candidate cerebellar folium to core for TMA production.

The 48 selected donor blocks were incubated at 37 °C overnight prior to core extraction. The Advanced Tissue Arrayer (VTA-100, Veridiam) was used to extract 2 mm tissue cores from the control and AD donor blocks (Narayan et al., 2015a). The coring site was selected based on assessment of the cresyl violet stained sections, which included the presence of a complete folium containing the molecular, Purkinje and granular cell layers. A single cerebellar folium ≤2 mm in total size was identified in each donor block, cored, and inserted into a blank recipient TMA paraffin block to form an array of cores. Once all donor cores had been extracted and inserted into the recipient TMA block, the block was incubated overnight at 37 °C, followed by 8 min incubation at 60 °C. This heating process allowed the paraffin between each core and the recipient paraffin block to anneal and amalgamate, allowing the cores to adhere to the recipient block. Once cooled to room temperature, the recipient block was cut into 7 μm thick sections serially using the paraffin microtome. Due to the varying core cylinder lengths within the recipient block (between 4 and 6 mm) which depended on the tissue thickness from the original donor blocks, only a subset of sections contained all 24 control and 24 AD cores. Approximately 100 sections were obtained from this TMA containing 20+ cores from control and 20+ cores from AD donor blocks. Each cut section was mounted serially onto positively charged slides within a hot water bath at 38–39 °C. Blank 2 mm cores that were inserted into the TMA within certain rows were used to ensure consistency in TMA section orientation during mounting. Once mounted and dried overnight at room temperature, the TMA sections were stored at room temperature until required for paraffin immunohistochemistry. The TMA used in this study is known as TMA 15.

2.3. Tissue microarray immunohistochemistry

Standard immunohistochemistry protocols were applied, as described previously (Waldvogel et al., 2007; Narayan et al., 2015a; Coppieters et al., 2014). A summary of primary, secondary, and tertiary antibodies, in addition to antigen retrieval protocols can be found in Table 5. The TMA sections were placed on a heating block at 60 °C for 1 h to anneal the mounted tissue onto the glass slide and aid paraffin dewaxing. The slides were subsequently dewaxed, via xylene immersion twice (1 h and 10 min respectively), and rehydrated in 100% ethanol twice for 5 min, followed by 2 min each in 95%, 80% and 75% ethanol and 3 washes in milliQ H_2O for 5 min. Heat-induced antigen retrieval was achieved through immersion in antigen retrieval buffer for 2 h at 121 °C in a pressure cooker (model 2100-retriever, Pick Cell

Table 2
Alzheimer's disease cases for cerebellum tissue microarray (TMA 15).

Case	Sex	Age at death (years)	Post-mortem delay (hours)	AD neuropathological grade[a]	Cause of death
AZ33	M	65	20	ARP: C	Hypostatic pneumonia
AZ34	F	74	18	ARP: C	Bronchopneumonia
AZ43	M	80	21	ARP: B	Bronchopneumonia
AZ46	F	82	22	ARP: B	Ischemic heart disease
AZ52	F	68	36	ARP: C	Bronchopneumonia
AZ55	M	51	4	ARP: B	Bronchopneumonia
AZ57	F	82	14.5	ARP: A	Bronchopneumonia
AZ58	M	75	20	ARP: C	Bronchopneumonia
AZ59	M	83	15	ARP: A	Cardiopulmonary collapse
AZ61	F	87	7.5	ARP: C	Bronchopneumonia
AZ62	F	80	11	ARP: C	Cachexia
AZ64	M	67	8	ARP: C	Bronchopneumonia
AZ68	F	68	7	ARP: C	Bronchopneumonia
AZ72	F	70	7	ARP: C BRAAK: V	Lung cancer
AZ78	F	87	7	ARP: B BRAAK: III	General inanition
AZ81	F	82	18	ARP: C BRAAK: VI	Respiratory failure
AZ82	F	80	18	ARP: C BRAAK: VI	Bronchopneumonia
AZ83	F	60	16	ARP: C BRAAK: VI	Bronchopneumonia
AZ87	M	73	5	ARP: C BRAAK: V	Bronchopneumonia
AZ89	F	80	25	ARP: C BRAAK: VI	Bronchopneumonia
AZ90	M	73	4	ARP: C BRAAK: IV	Gastrointestinal haemorrhage
AZ93	M	83	15	ARP: C BRAAK: V	Bronchopneumonia
AZ96	F	74	8.5	ARP: C BRAAK: V	Metastatic cancer (gut)
AZ101	M	75	12.5	BRAAK: VI	Bronchopneumonia
Mean	14F/10M	75.0	14.2		
Standard deviation		8.8	7.8		

F = female; M = male.

[a] AD pathological grades were designated with an age-related plaque (ARP) score with "A" reflecting low number of plaques and "C" reflecting a high number of plaques; or BRAAK staging with "III" reflecting the pathological presence of neurofibrillary tangles in the entorhinal, transentorhinal, limbic allocortex and adjoining neocortex, and "VI" reflecting the presence of tangles in all aforementioned areas, in addition to the wider neocortex including the secondary and primary fields.

Table 3
Neurologically normal control cases for cerebellar whole-section analysis.

Case	Sex	Age at death (years)	Post-mortem delay (hours)	Cause of death
H108	M	58	16	Coronary atherosclerosis
H111	M	46	10	Coronary artery disease
H118	M	57	10	Coronary artery disease
H119	M	58	15	Ischaemic heart disease
H124	M	49	13	Ischaemic heart disease
H132	F	63	12	Ruptured aorta
Mean	1F/5M	55.2	12.7	
Standard deviation		6.4	2.5	

Laboratories). For tau and amyloid-β immunohistochemistry, once the slides had cooled post-antigen retrieval, an additional incubation in 99% formic acid was carried out for 5 min followed by 3 washes in milliQ H_2O.

Endogenous peroxidases were quenched with a 20 min incubation in endogenous peroxidase blocking solution (50% methanol, 1% H_2O_2, diluted in milliQ H_2O) at room temperature. The slides were subsequently washed 3 times in PBS (phosphate-buffered saline) before exposure to a blocking buffer (either 10% normal goat or donkey serum in PBS) for 1 h at room temperature. Post serum block, the slides were incubated with the primary antibodies overnight at 4 °C. The following day, the slides were washed first in PBS-T (phosphate-buffered saline with 0.2% Triton X-100) for 5 min, and twice in PBS for 5 min each, before the secondary antibody incubation was performed for 3 h at room temperature. The slides were washed again before the ExtrAvidin peroxidase (Sigma, 1:1000) incubation was carried out for 1 h at room temperature. Another washing step was conducted before incubating the slides in the peroxidase substrate (0.5% 3,3′-diaminobenzidine (DAB)), 0.01% H_2O_2 intensified with 0.04% nickel ammonium sulfate until the colour reaction was visible. The peroxidase substrate was washed off using PBS and milliQ H_2O (3 times, 5 min each for both PBS and milliQ H_2O). The slides were dehydrated (2 min each in 75%, 80% and 95% ethanol, 5 min in 100% ethanol twice, and three times in xylene for 10 min each) before applying a coverslip using DPX mounting medium (Merck). The blocking, antibody and ExtrAvidin incubations were performed in a humidity chamber to prevent sections from drying out. Antibodies and ExtrAvidin were diluted in goat or donkey immunobuffer (1% normal goat or donkey serum in PBS). No-

Table 4
Alzheimer's disease cases for cerebellar whole-section analysis.

Case	Sex	Age at death (years)	Post-mortem delay (hours)	AD neuropathological grade[a]	Cause of death
AZ58	M	75	20	ARP: C	Bronchopneumonia
AZ64	M	67	8	ARP: C	Bronchopneumonia
AZ82	F	80	18	ARP: C BRAAK: VI	Bronchopneumonia
AZ87	M	73	5	ARP: C BRAAK: V	Bronchopneumonia
AZ93	M	83	15	ARP: C BRAAK: V	Bronchopneumonia
AZ101	M	75	12.5	BRAAK: VI	Bronchopneumonia
Mean	1F/5M	75.5	13.1		
Standard deviation		5.6	5.8		

F = female; M = male.
[a] All AD cases selected had advanced AD pathology, represented with an age-related plaque (ARP) score of "C" reflecting a high number of plaques; or BRAAK staging of V-VI reflecting widespread neurofibrillary tangles (severe AD pathology).

primary controls, where the primary antibody is omitted from the immunobuffer was performed for each antibody to assess the degree of nonspecific labelling due to the secondary antibody.

2.4. Free-floating immunohistochemistry

To validate significant findings from the cerebellar TMA, free-floating immunohistochemistry was conducted on 3 neocerebellar sections (a lateral, middle and medial section) obtained from block CB1 from $n = 6$ control and n = 6 AD cases (Tables 3 and 4) using standard single peroxidase labelling techniques as detailed previously (Waldvogel et al., 2007; Coppieters et al., 2014; Narayan et al., 2015b). Briefly, 50 μm cut sagittal neocerebellar sections were permeabilized in PBS-T overnight at 4 °C in six-well tissue culture plates. Upon PBST removal, the sections were immersed in antigen retrieval buffer and placed into a 650 watts microwave oven for 40 s (until boiling) and allowed to cool at room temperature. Endogenous peroxidases were quenched with a 30 min incubation in 50% methanol, 1% H_2O_2, diluted in milliQ H_2O at room temperature. Sections were incubated in primary antibodies for 3 days at 4 °C. Sections were subsequently incubated with the corresponding biotinylated secondary antibody overnight at room temperature, followed by ExtrAvidin peroxidase for 4 h at room temperature. Finally, the sections were incubated in 0.5% 3,3′-diaminobenzidine, 0.01% H_2O_2 intensified with 0.04% nickel ammonium sulfate until the colour reaction was visible (10–20 min). The sections were carefully mounted in gelatin onto slides, allowed to dry for 1–2 days before dehydration through the following series: 5 min in 75%, 85% and 95% ethanol, 10 min in two lots of 100% ethanol, and three 20 min immersions in xylene before being coverslipped with DPX mounting medium (Merck). A no-primary antibody condition was used as a negative control for each antibody. Three 10 min washes were conducted with PBS-T between every step post-antigen retrieval. Antibodies and ExtrAvidin peroxidase incubations were diluted in goat or donkey immunobuffer (1% normal goat/donkey serum in PBS-T containing 0.04% thimerosal). The antibodies in this present study have been widely used, and their specificities have been previously validated by western blotting, immunocytochemistry and immunohistochemistry in human tissue by independent researchers (Table 5).

2.5. Image acquisition

Images were acquired for each immunolabelled TMA slide using a VSlide automated slide scanning microscope (Metasystems) running Metafer4 software (version 3.12.133) utilising a TMA imaging protocol outlined by Narayan et al. (2015a). Briefly, an initial automated low-power pre-scan of the TMA was generated using a 2.5× objective lens. The pre-scan image was opened using the 'Microarray Tool' function within Metafer4 software, and threshold based segmentation was performed to localise the immunolabelled cores. A 6 × 10 grid of interconnected 'dots' were placed over the thresholded cores, and each 'dot' was manually placed in the centre of each core of interest. Once the centre of each core was finalised, a subsequent automated re-scan was carried out for each core at 10× magnification across the entire TMA in a high-throughput, standardised fashion. Four images were acquired around the centre for each core in order to capture the entire 2 mm core with sufficient detail. Images acquired were automatically saved with individual filenames corresponding to the core coordinates. The re-scan images were inspected for cores containing folded, missing, or torn tissue which were excluded from subsequent analysis.

Whole neocerebellar sections were imaged using the 'Rescan Region of Interest (ROI)' setting of the VSlide scanner running Metafer4 software. In brief, a slide size of 76 × 60 mm was selected, and a pre-scan of the whole slide was generated using a 2.5× objective lens. The pre-scan image was automatically stitched together and saved into a 'MetaClient' directory. The image was reopened with Metaviewer, where contours were drawn over the stitched pre-scan to delineate the ROI for a higher resolution re-scan. The ROI included all cerebellar branches to capture every folium within the sagittal section. Once the contour was complete, the ROI was re-scanned automatically using a 10× objective lens, resulting in 1000–2000 images captured within the defined ROIs per slide. The re-scan images were manually scrutinised, and images with folded, torn, or absent cerebellar folia were excluded from analysis.

2.6. Image analysis using high-content screening

The images acquired were analysed using Metamorph software (Metamorph Offline v.7.8.0, Molecular Devices). Image analysis for the TMA cores were conducted using the 'Count Nuclei algorithm' (Narayan and Dragunow, 2010). For each immunolabel, Count Nuclei measurements logged within an excel spreadsheet included the following: total nuclei (if cells were quantified), total area (of the immunolabel) and integrated intensity. In addition, the whole area of each core was determined using the 'Threshold Image' command. Thresholding applied segmentation to an image by taking objects of interest (in this case, the whole core) that were above a pre-defined grayscale value. Once the core was isolated, the thresholded area was logged using the 'Show Region Statistics' function. Therefore, TMA data for each immunolabel presented here includes the integrated intensity (total intensity of immunolabel) and load (area of immunolabel as a percentage of total area of the core) expressed as a mean of 4 images per core. For CD31 vessel quantification, a custom analysis workflow was created to quantify longitudinal and transverse vessels. The workflow identified vascular staining that met user-defined size and intensity criteria; the Adaptive Threshold tool was used to measure the area and integrated intensity of all vessel staining; the Angiogenesis Tube Formation tool quantified

Table 5
Antibodies and conditions used to study the Alzheimer's cerebellum.

Antigen	Host	Concentration for TMA immunohistochemistry	Concentration for free-floating immunohistochemistry	Company	Catalogue number	Antigen retrieval buffer	References for antibody specificity in human tissue western blots and immunohistochemistry	Secondary and tertiary antibody details
Amyloid-β	Mouse	1:100		DAKO	M0872	Citrate pH 6 + formic acid	(Adams et al., 2016) (Montine et al., 2016) (Narayan et al., 2015b) (Coppieters et al., 2014)	Goat anti-mouse IgG Sigma B7264 dilution 1:500 for TMA and 1:1000 for free-floating; ExtrAvidin Sigma E2886 dilution 1:1000; DAB-nickel
Ubiquitin	Mouse	1:2000		Millipore	MAB1510	Citrate pH 6	(Narayan et al., 2015b) (Coppieters et al., 2014) (Neumann et al., 2006) (Furukawa et al., 2004) (Spillantini et al., 1998)	
α-SMA	Mouse	1:2		DAKO	IS611	Citrate pH 6	(Jansson et al., 2016)	
CD31/ PECAM-1	Mouse	1:20	1:500	DAKO	M0823	Tris-EDTA pH 9	(Stokum et al., 2015) (Lowe et al., 2015) (Xue et al., 2015) (Nakayama et al., 2010)	
HLA-DP, DQ, DR (MHC II) (clone CR3/43)	Mouse	1:100	1:5000	DAKO	M0775	Tris-EDTA pH 9	(Narayan et al., 2015b) (Serrano-Pozo et al., 2013) (Smith et al., 2013) (Haider et al., 2011)	
GFAP	Mouse	1:5000		Sigma	G3893	Citrate pH 6	(Narayan et al., 2015b) (Coppieters et al., 2014) (Smith et al., 2013)	
Calbindin	Rabbit	1:5000		Swant	CB38a	Citrate pH 6	(Gottardi et al., 2016) (Whitney et al., 2008)	Goat anti-rabbit IgG Sigma B7389 dilution 1:500 for TMA and 1:2500 for free-floating; ExtrAvidin Sigma E2886 dilution 1:1000; DAB-nickel
Fibronectin	Rabbit	1:1000	1:2500	DAKO	A0245	Citrate pH 6	(Rustenhoven et al., 2015) (Dragunow et al., 2016)	
PDGFRβ [Y92]	Rabbit	1:50		Abcam	Ab32570	Citrate pH 6	(Dieriks et al., 2017) (Cisbani et al., 2013)	
Collagen IV	Rabbit	1:100		Abcam	Ab6586	Citrate pH 6	(Garbuzova-Davis et al., 2013) (Moore et al., 2016) (Keable et al., 2016)	
Human Tau	Rabbit	1:10,000		DAKO	A0024	Citrate pH 6 + formic acid	(Kurbatskaya et al., 2016) (Narayan et al., 2015b) (Coppieters et al., 2014)	
IBA-1	Goat	1:1000	1:2500	Abcam	Ab5076	Tris-EDTA pH 9	(Zhou et al., 2015) (Coppieters et al., 2014) (Smith et al., 2013)	Donkey anti-goat IgG Jackson Immuno Research 705–065-003 dilution 1:5000 for TMA and free-floating; ExtrAvidin Sigma E2886 dilution 1:1000; DAB-nickel

longitudinal vessels and associated branch points; the Count Nuclei tool counted transverse vessels in images from which the longitudinal vessels were subtracted. All measurements were normalised to the total imaged area for that core.

Analysis for whole cerebellar sections immunolabelled with free-floating immunohistochemistry were conducted using the same Metamorph journals as described for TMA analysis. However, integrated intensities which we found to alter in AD sections were also re-plotted as integrated intensity per immunopositive cell to account for variability in cell number between control and AD cases (Coppieters et al., 2014). In addition, for microglial morphology measurements within sections (IBA1 and HLA-DR), the 'Neurite Outgrowth' module was used to generate segmentation masks specific for IBA1 and HLA-DR immunolabels (Narayan et al., 2015a). The Neurite Outgrowth measurements logged included: mean outgrowth per cell, mean processes per cell and mean branches per cell. The data for whole sections were presented as a mean of all images quantified per case.

2.7. Statistical analysis

Data obtained from the Metamorph software were statistically analysed using GraphPad Prism (version 7.03). The mean AD and control data from TMA and whole section validation were screened for normality and homoscedasticity. Normality was graphically assessed using a dot plot of the data, where the data was considered to be normal if 95% of data points fell within two standard deviations of the mean. The D'Agostino-Pearson omnibus test also assessed normality using GraphPad Prism. Data was considered normally distributed if $p < 0.05$. The Brown-Forsythe test assessed homoscedasticity, where $p < 0.05$ was considered to be groups with unequal variances. Based on dot plot screening, normality and homoscedasticity tests, the majority of the control and AD TMA data for each immunolabel were from a Gaussian population. Therefore, the comparisons between AD and control groups for TMA data were conducted using a 2-tailed Student's unpaired *t*-test with Welch's correction for unequal variances. Subgroup comparisons within the AD and control groups (such as gender comparisons) utilized Kruskal–Wallis test combined with Dunn's multiple comparisons post-test due to departures from normality. The control and AD data analysed from free-floating whole sections were compared using a 2-tailed Mann-Whitney test due to departures from normality and unequal variances. A *p*-value ≤ 0.05 was considered statistically significant ($^{*}p \leq 0.05$, $^{**}p \leq 0.01$, $^{***}p \leq 0.001$). Results were presented as mean ± standard deviation.

3. Results

3.1. Extent of cerebellar neuropathology in AD

The results of tissue microarray (TMA) analysis demonstrated a significant increase in amyloid-β (Aβ) expression and coverage within the AD cerebellum (Fig. 2a-d), with a 433% increase in Aβ integrated intensity ($p = 0.01$) and 1482% increase in load ($p = 0.007$). In comparison, TMA analysis of tau expression and coverage (Fig. 2e-f) indicated no significant differences between AD and control cohorts. However, a small subset of AD cases with tau-positive circular-shaped staining (Fig. 2h) are represented as outliers in Fig. 2e-f. TMA analysis of ubiquitin (Fig. 2i-l) in AD compared with control cores demonstrated no significant differences in expression and coverage. To assess Purkinje cells in the cerebellum (Fig. 2m-p), TMA analysis of cell number and expression of calbindin-positive Purkinje cell bodies revealed no differences between the AD and control cohorts.

3.2. Increase in IBA1 expression and altered IBA1 microglial morphology in AD neocerebellum tissue

TMA analysis of IBA1 microglia revealed a significant increase in expression and coverage within AD cerebellar cores (Fig. 3a-b), with a 91% increase in integrated intensity ($p = 0.002$) and 69% increase in load ($p = 0.01$). To understand the contribution of cellular morphology and cell number to the increased cerebellar IBA1 expression in AD TMAs, 1000–2000 images were analysed from 3 whole neocerebellar sections from control ($n = 6$) and AD ($n = 6$) cases (Fig. 3c-f). No significant differences in IBA1 microglial cell number (Fig. 3c) was found between the control and AD cases, which suggests that the elevation in IBA1 expression and coverage is not attributable to differences in cell number. However, IBA1 expression in these whole sections normalised to cell number to give IBA1 integrated intensity per cell was significantly increased by 27% ($p = 0.03$) in AD, thus reinforcing greater IBA1 expression within individual IBA1-positive microglia (Fig. 3d). Quantitative (Fig. 3e-f) examination of IBA1-positive microglial morphology in whole neocerebellar sections revealed a significant reduction in process length per cell (22% reduction, $p = 0.03$) and branches per cell (41% reduction, $p = 0.03$) within the AD cases. AD IBA1-positive microglia appear to be less ramified (Fig. 3g-h), possess fewer branches, and widely appear hypertrophic compared to control microglia.

3.3. Presence of deramified dystrophic HLA-DR-positive microglia in AD neocerebellum tissue

TMA analysis revealed no significant changes in HLA-DR expression or coverage (Fig. 4a-b). Subsequent HLA-DR cell counts were conducted for 1000–2000 images obtained from 3 neocerebellar sections for control ($n = 6$) and AD ($n = 6$) cases (Fig. 4c), revealing no differences in HLA-DR-positive microglial cell number. Quantitative (Fig. 4d-e) examination of HLA-DR-positive microglial morphology in whole neocerebellar sections revealed a significant reduction in process length per cell (33% reduction, $p = 0.009$) and branches per cell (49% reduction, $p = 0.004$) within the AD cases. HLA-DR-positive microglia within the AD neocerebellum showed considerable abnormalities compared to control cases (Fig. 4f-g), with shortened, fragmented, deramified and beaded processes, indicating that they are dystrophic.

3.4. Absence of GFAP astrocytic changes in AD neocerebellum tissue

TMA analysis revealed no significant changes in GFAP expression or coverage in AD (Fig. 5a-b). GFAP immunoreactivity was extensive within both control and AD neocerebellar folia (Fig. 5c-d), with abundant fibrous staining, particularly within the granule cell layer, which made the identification of cell bodies difficult for any further quantification. Closer examination of GFAP-positive astrocytes (insets, Fig. 5c-d) showed similar morphologies in the AD and control folia, suggestive of a resting astrocytic phenotype and an absence of astrogliosis in the AD cerebellum.

3.5. Increase in vascular fibronectin in AD neocerebellum tissue with no change in collagen IV

TMA analysis of vascular fibronectin expression (Fig. 6a) revealed a significant 27% increase in integrated intensity ($p = 0.04$) in AD cerebellar cores, with no change in overall fibronectin load (Fig. 6b). Qualitative examination of fibronectin immunoreactivity within the cerebellar molecular layer of whole cerebellar sections reinforces the TMA data (Fig. 6c-f) with more intense immunoreactivity throughout AD capillaries compared to control cases. TMA analysis of collagen IV (Additional file 1: Supplementary Fig. 1a-d) in AD compared with control cores demonstrated no significant differences in expression and coverage.

3.6. Greater number of CD31 vessels in AD neocerebellum tissue

TMA analysis of vascular CD31 demonstrated a significant increase

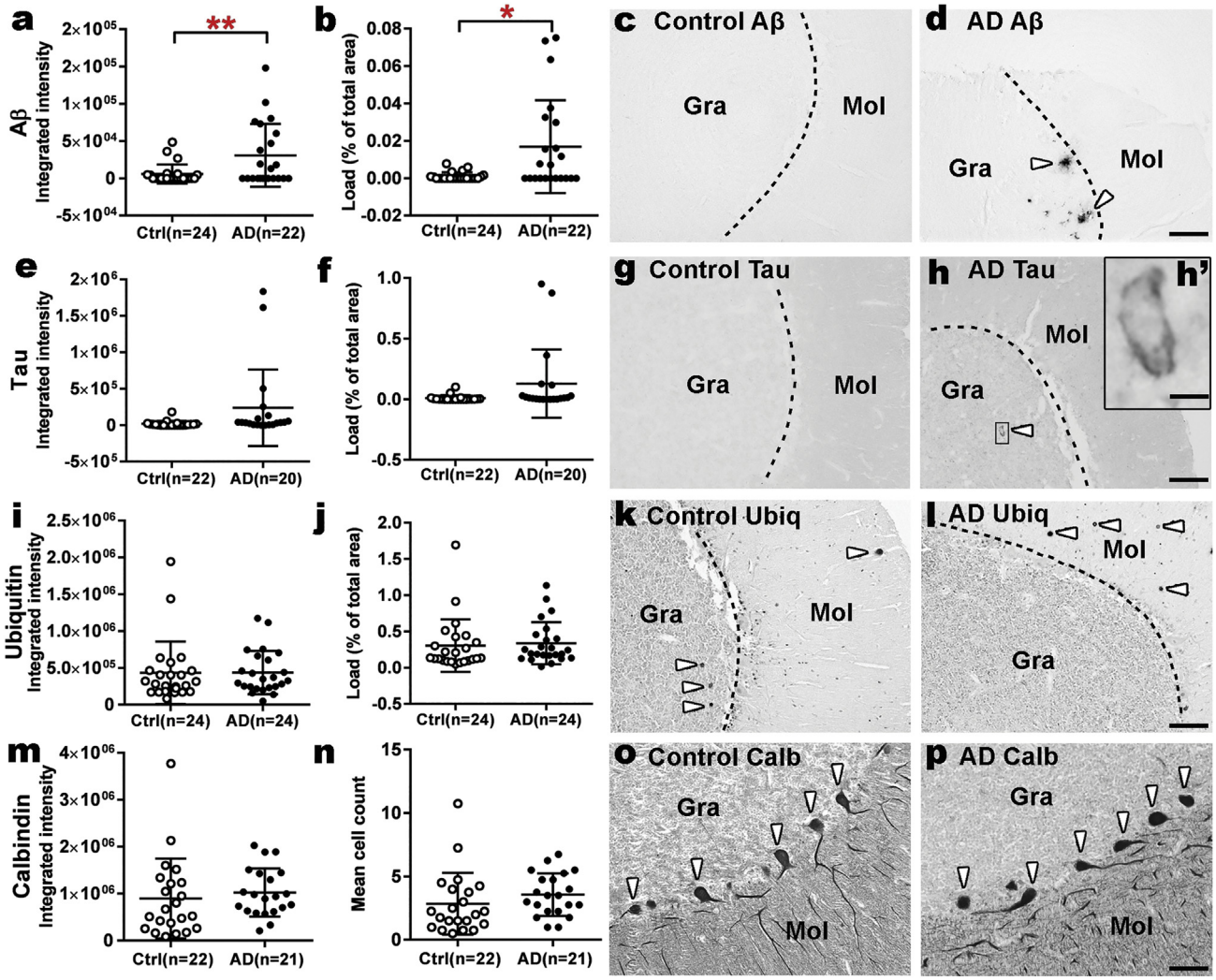

Fig. 2. Quantification of Aβ, tau, ubiquitin and calbindin immunoreactivity in control and AD cerebellar tissue microarray cases. Integrated intensity and load measurements were used to quantify the AD neuropathological hallmarks (a-d) Aβ, (e-h) tau, and (i-l) ubiquitin levels in TMA 15. A significant increase in Aβ levels were found in AD (n = 22) compared to control (n = 24) cases, evidenced by (a) a 433% increase in Aβ integrated intensity (p = 0.01) and (b) a 1482% increase in Aβ load (p = 0.007). (c-d) Photomicrographs of TMA paraffin cores from (c) representative control case H239 and (d) AD case AZ46. White arrowheads denote the presence of Aβ plaques. No significant differences were observed in tau immunoreactivity between control (n = 22) and AD (n = 20) in terms of tau (e) integrated intensity (p = 0.076) and (f) load (p = 0.074). No Tau immunoreactivity was identified within control TMA paraffin cores, as illustrated in (g) representative control case H123. A small subset of AD cases contained tau-positive circular structures (h) as demonstrated with a white arrowhead in representative AD case AZ101. A high power inset of (h') tau-positive immunoreactivity within the granule cell layer of AD case AZ101 illustrates the unusual doughnut-shape appearance of the structure. No tau-positive neurofibrillary tangles were identified within the AD cores examined. No differences were observed in ubiquitin immunoreactivity between control (n = 24) and AD (n = 24) cases in terms of ubiquitin (i) integrated intensity (p = 0.99) and (j) load (p = 0.73). Ubiquitin immunoreactivity was identified in photomicrographs of control and AD TMA paraffin cores, denoted with white arrows in (k) representative control case H239 and (l) AD case AZ46. To assess Purkinje cells in TMA 15, calbindin immunoreactivity (m-p) was quantified. No differences were observed in calbindin (m) integrated intensity (p = 0.55) or (n) calbindin-positive Purkinje cell counts (p = 0.27) between control (n = 22) and AD (n = 21) cases. (o-p) Photomicrographs of TMA paraffin cores from (o) representative control case H239 and (p) AD case AZ58. White arrows denote the presence of calbindin-positive Purkinje cell bodies. Significance values are based on p-values from a two-tailed unpaired t-test with Welch's correction for unequal variance. *p < 0.05, **p < 0.01. Scale bar corresponds to 100 μm in c-d, g-h, k-l, o-p and 10 μm in h'. Ctrl = control; AD = Alzheimer's disease; Ubiq = Ubiquitin; Calb = Calbindin; Gra = granule cell layer; Mol = molecular cell layer.

in CD31 expression and coverage within the AD cerebellum (Fig. 7a-b), with a 114% increase in CD31 integrated intensity (p = 0.006) and 115% increase in load (p = 0.001). To investigate the relative contributions of vessel number and CD31 expression per vessel to the increase in CD31 integrated intensity, the number of CD31 vessels were quantified and the expression of CD31 was reanalyzed and normalised to vessel number (Fig. 7c-d). The number of CD31-positive vessels was found to be significantly increased by 98% (p = 0.02) in AD cases relative to controls (Fig. 7c). Normalizing the expression of CD31 to vessel number revealed no significant differences between control and AD cores (Fig. 7d), which reinforces that the greater expression and coverage of CD31 in the AD neocerebellum is attributable to a greater number of vessels in AD. Qualitative examination of CD31 immunoreactivity within the cerebellar molecular layer of whole sections reinforces the TMA data (Fig. 7e-f) with considerably greater numbers of CD31-positive vessels present in the AD neocerebellum relative to controls.

3.7. No change in mural cells in AD neocerebellum tissue

TMA analysis of mural cell markers platelet-derived growth factor receptor beta (PDGFRβ) and alpha smooth muscle actin (αSMA) in AD compared with control cases demonstrated no significant differences in overall expression or coverage (Additional file 1: Supplementary

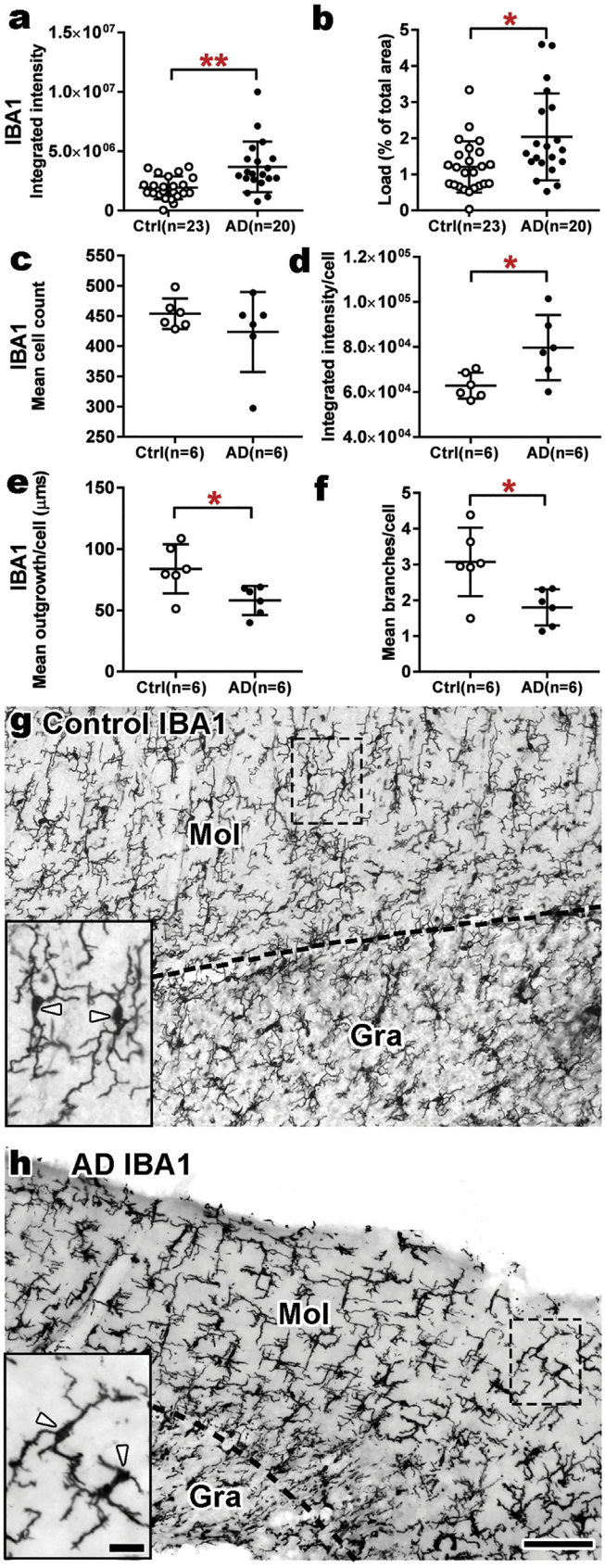

Fig. 3. Increase in IBA1 expression and altered IBA1-positive microglial morphology in AD neocerebellum tissue. (a-b) IBA1 levels were found to be significantly elevated in AD (n = 20) compared to control (n = 23) cases in TMA 15, evidenced by (a) a 91% increase in IBA1 integrated intensity (p = .002) and (b) 69% increase in IBA1 load (p = 0.01). (c-f) Whole section analysis was conducted for IBA1 immunoreactivity in 3 neocerebellar sections from control (n = 6) and AD (n = 6) cases. (c) IBA1-positive soma quantification revealed no differences between control and AD cases (p = 0.39). (d) Integrated intensity per IBA1-immunopositive cell significantly increased by 27% (p = 0.03), suggesting elevated protein expression per cell within the AD cerebellum. (e) Measurements of IBA1-positive microglia process length revealed a 22% reduction in length per cell in AD (p = 0.03) compared to controls. (f) Quantification of IBA1 microglial branches demonstrates a 41% reduction in branching number per cell in AD (p = 0.03) compared to controls. (g-h) Representative photomicrographs of IBA1 immunoreactivity in free-floating neocerebellar sections from (g) control case H119 and (h) AD case AZ64 demonstrate elevated IBA1 staining intensity and altered morphologies of IBA1-positive microglia in AD. Closer examination of IBA1-positive microglia (soma denoted with white arrows in insets of g-h) illustrates differences in morphology in AD, such as cells being less ramified, possessing fewer branches with retracting processes and widely appearing hypertrophic compared to the ramified microglia in control tissue. Significance values for a-b are based on p-values from a two-tailed unpaired t-test with Welch's correction for unequal variance. Significance values for c-f are based on a non-parametric two-tailed unpaired Mann-Whitney test. *$p < 0.05$, **$p < 0.01$. Scale bar corresponds to 100 µm in g-h and 20 µm for insets. Ctrl = control; AD = Alzheimer's disease; Gra = granule cell layer; Mol = molecular cell layer; IBA1 = anti-ionized calcium-binding adaptor molecule 1.

Fig. 1e-l). However, given the identified increase in vessel number in AD, the ratio of PDGFRβ to CD31 load between the AD and control group was also analysed (Fig. 7i). The PDGFRβ:CD31 load ratio was found to be significantly reduced by 59% (p = 0.005) in AD cases relative to controls, which suggests there is less PDGFRβ per CD31-positive vessel in AD, perhaps reflective of decreased pericyte coverage of neovascular structures in AD.

4. Discussion

This study is the first to document microglial and neurovascular perturbation without the overt loss of Purkinje cells in the AD neocerebellum. This study utilized high-content analysis methods of neuropathology, glia and neurovascular features on human neocerebellar tissue microarrays (TMAs) from 24 AD and 24 matched control cases. These data were validated by repeating the analysis in thicker free-floating whole sections (3 per case) from 6 AD and 6 control cases. Our results also support the notion that microglial phenotypic change, rather than proliferation, underlies microglial responses in the AD neocerebellum. Furthermore, we provide preliminary evidence of basement membrane-associated extracellular matrix molecular involvement in neocerebellar AD pathogenesis. Finally, we provide evidence to suggest that more CD31/PECAM-1-positive blood vessels are present within the AD neocerebellum, which may impact the ratio of perivascular PDGFRβ to CD31, and ultimately the patency of the vessels. These findings provide evidence that AD-related molecular changes occur within non-neuronal cells of the neocerebellum, which may contribute to the symptomatology and pathophysiology of AD.

4.1. Tissue microarray documentation recapitulates neocerebellar neuropathology in AD

Our study of neocerebellar neuropathology using TMAs revealed a considerable increase in amyloid-β expression and load within AD cases, which is in general agreement with earlier studies of AD neuropathology (Braak et al., 1989; Joachim et al., 1989; Dickson et al., 1990; Li et al., 1994; Fukutani et al., 1997; Wegiel et al., 1999; Wang et al., 2002). Furthermore, no tau-positive neurofibrillary tangles were

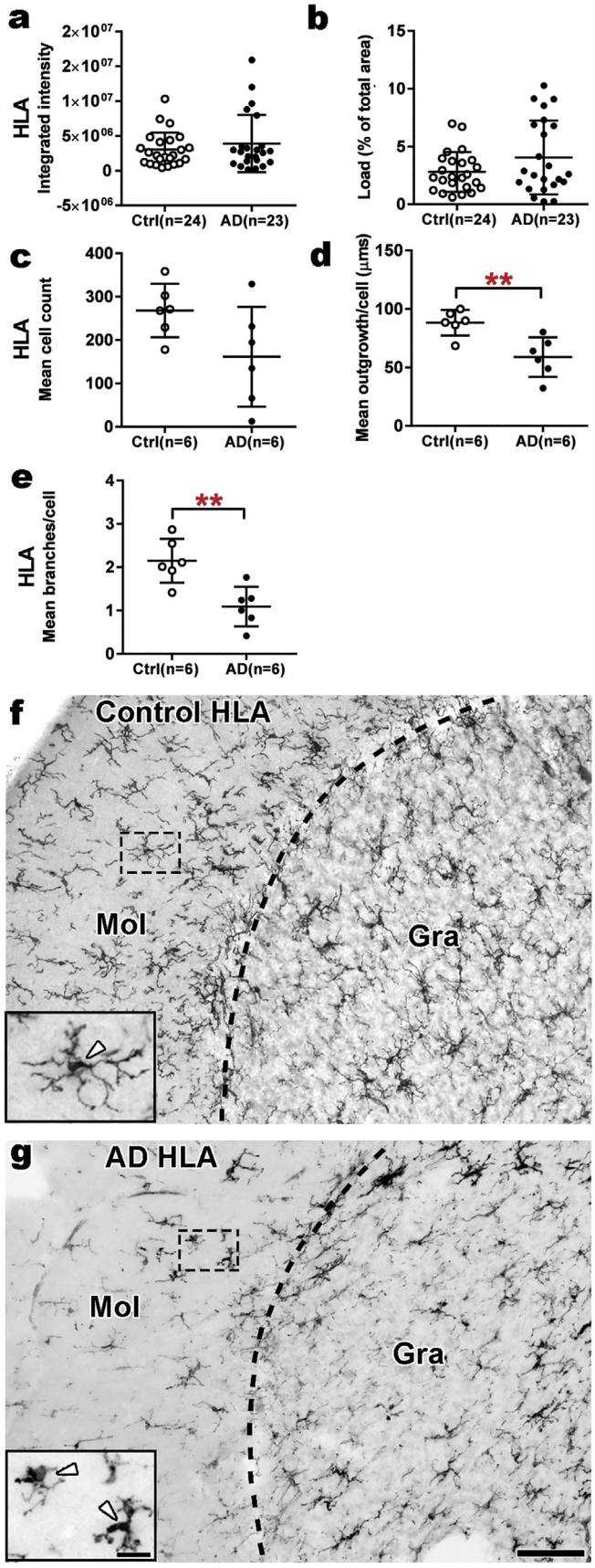

Fig. 4. Presence of deramified dystrophic HLA-DR-positive microglia in AD neocerebellum tissue. (a-b) Integrated intensity and load measurements were used to quantify microglial HLA-DR immunoreactivity in control (n = 24) and AD (n = 23) cases within TMA15. No changes in HLA-DR expression were observed in terms of (a) integrated intensity (ns; p = 0.39) and (b) load (ns; $p = 0.11$). (c-e) Whole section analysis was conducted for HLA-DR immunoreactivity in 3 neocerebellar sections from control (n = 6) and AD (n = 6) cases. (c) HLA-DR-positive soma quantification revealed no differences between control and AD cases ($p = 0.13$). (d) Measurements of HLA-DR microglia process length revealed a 33% reduction in length per cell in AD ($p = 0.009$) compared to controls. (e) Quantification of HLA-DR-positive microglial branches demonstrates a 49% reduction in branching number per cell in AD ($p = 0.004$) compared to controls. (f-g) Representative photomicrographs of HLA-DR immunoreactivity in free-floating neocerebellar sections from (f) control case H119 and (g) AD case AZ64 demonstrate the abnormal morphology of HLA-DR-positive microglia in AD. Closer examination of HLA-DR positive microglia in AD compared to controls (soma denoted with white arrows in insets of f-g) illustrates shortened, fragmented, deramified and beaded processes, reflecting the appearance of dystrophic HLA-DR microglia in AD. Significance values for a-b are based on p-values from a two-tailed unpaired t-test with Welch's correction for unequal variance. Significance values for c-f are based on a non-parametric two-tailed unpaired Mann-Whitney test. *p < 0.05, **p < 0.01. Scale bar corresponds to 100 µm in f-g and 20 µm for insets. Ctrl = control; AD = Alzheimer's disease; Gra = granule cell layer; Mol = molecular cell layer; HLA = HLA, human leukocyte antigen.

identified in AD neocerebellar TMA cores, which is in line with previous observations (Joachim et al., 1989; Li et al., 1994; Wegiel et al., 1999; Yamamoto and Hirano, 1985). However, a small subset of AD cases contained tau-positive circular structures, which could be investigated in future studies to determine the cellular localisation and nature of these structures. Ubiquitin immunoreactivity was identified in both control and AD cores, however, unlike the AD cerebral cortex, ubiquitin was not elevated in the human AD neocerebellum, which widely agrees with previous observations in human tissue (Wang et al., 1991). A possible explanation for a lack of ubiquitin elevation in the neocerebellum in AD is the absence of neurofibrillary tangles which tend to be decorated with ubiquitin, combined with a lack of proteosomal activity impairment as previously reported in the cerebellum in AD (Keller et al., 2000; Ihara et al., 2012). In terms of Purkinje cell numbers in AD, the preservation of cells in our neocerebellar TMA is consistent with recent investigations of Purkinje cells, including a design-based stereological study conducted in 10 AD compared with 10 control cerebella (Andersen et al., 2012; Stępień et al., 2012). Taken together, our data detailing a significant increase in neocerebellar amyloid-β, with no significant changes in tau, ubiquitin, and Purkinje cell numbers analysed in human TMAs recapitulate cerebellar neuropathology previously reported in several studies investigating whole neocerebellar sections. These data justify the rationale of using the TMA approach to investigate other components implicated in the pathogenesis of AD in a tissue-conserving manner, such as the contribution of glial cells and neurovasculature.

4.2. Perturbed microglia within AD neocerebellum consists of phenotypic change, not proliferation

Ionized calcium-binding adaptor molecule 1 (IBA1) is a microglial cytoplasmic protein (Imai et al., 1996). Although IBA1 expression is believed to increase with microglial activation (Ito et al., 1998) where it may be involved in membrane ruffling, phagocytosis and cell mobility (Ohsawa et al., 2000; Ito et al., 2001; Ito et al., 1998; Sasaki et al., 2001), it is widely considered a pan-marker for microglia, rather than an activated subpopulation (Walker and Lue, 2015). A recent systematic review summarised the results of twenty papers quantitatively comparing IBA1 between control and AD post-mortem human brains, and it is quite evident that our study is the first to quantitatively compare IBA1 between control and AD neocerebellum (Hopperton

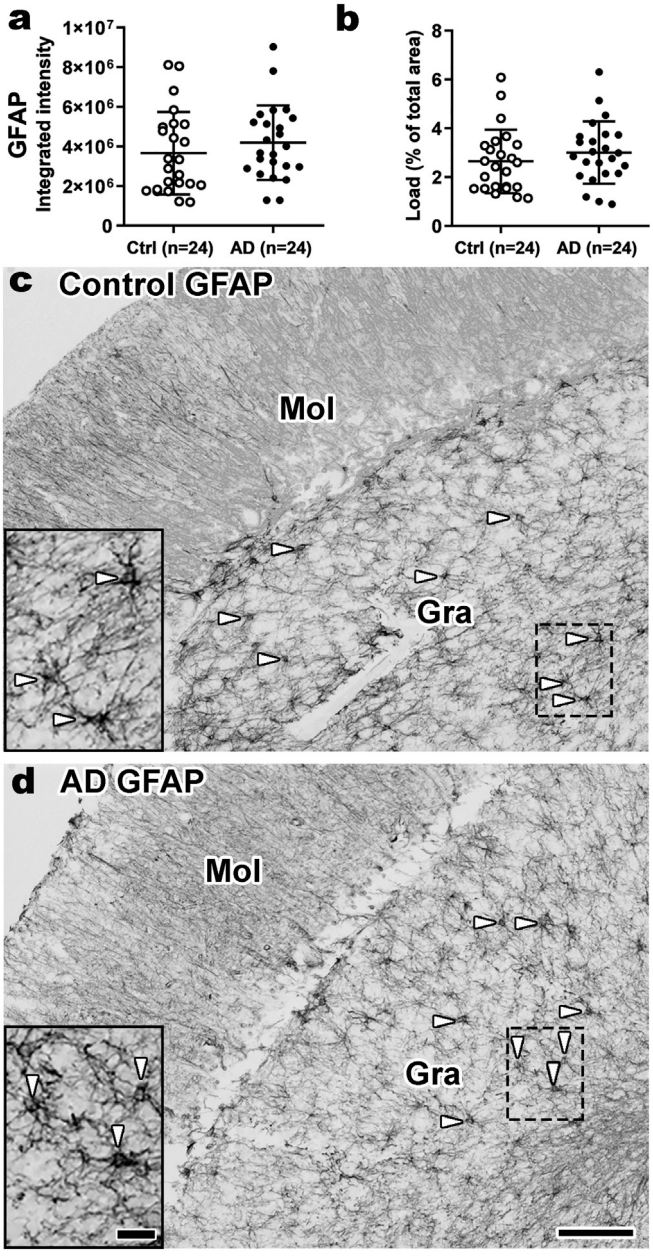

Fig. 5. Quantification of GFAP immunoreactivity in control and AD cerebellar tissue microarray cases demonstrate an absence of astrocytosis in AD. (a-b) Integrated intensity and load measurements were used to quantify GFAP immunoreactivity in control (n = 24) and AD (n = 24) cases within TMA15. No significant differences were observed in GFAP immunoreactivity between control and AD cases in terms of (a) integrated intensity ($p = 0.36$) and (b) load ($p = 0.34$). GFAP immunoreactivity was identified in photomicrographs of control and AD TMA paraffin cores, with cell bodies denoted with white arrows in (c) representative control case H148 and (d) AD case AZ57. Closer examination of GFAP-positive astrocytes in AD compared to control cases (soma denoted with white arrows in insets of c-d) illustrates no visible soma hypertrophy or thickening of processes within the AD neocerebellar granule cell layer, suggesting an absence of astrocytosis. Significance values for a-b are based on p-values from a two-tailed unpaired t-test with Welch's correction for unequal variance. Scale bar corresponds to 100 μm in c-d and 20 μm for insets. Ctrl = control; AD = Alzheimer's disease; Gra = granule cell layer; Mol = molecular cell layer; GFAP = Glial fibrillary acidic protein.

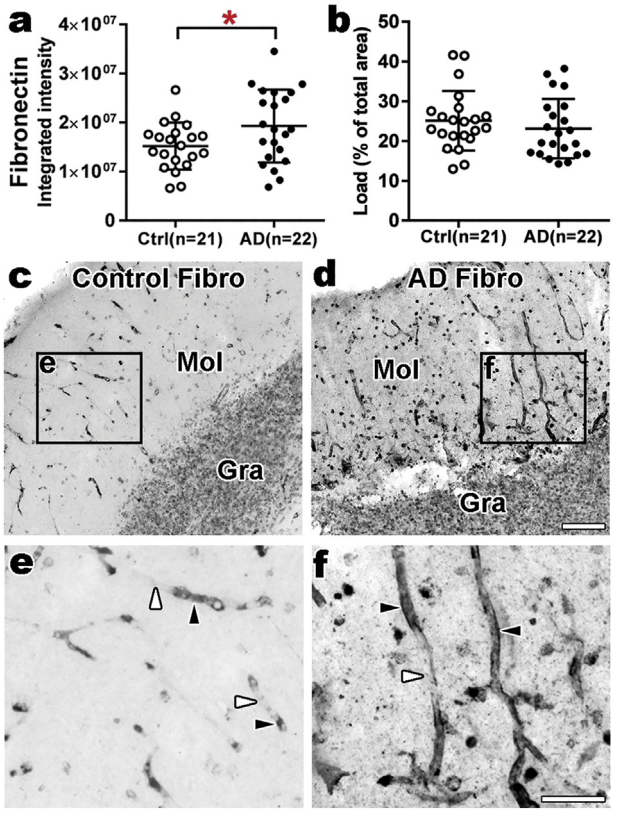

Fig. 6. Increase in vascular fibronectin in AD neocerebellum tissue. (a-b) Integrated intensity and load measurements were used to quantify fibronectin immunoreactivity in control ($n = 21$) and AD (n = 22) cases within TMA15. (a) A significant 27% increase in fibronectin integrated intensity ($p = 0.04$) was found in AD TMA cores compared to control cores. (b) No changes in fibronectin load (ns; $p = 0.38$) were found. (c-d) Representative photomicrographs of fibronectin immunoreactivity in free-floating neocerebellar sections from (c) control case H119 and (d) AD case AZ64 illustrate the higher intensity of immunoreactivity within the molecular layer in AD. (e-f) Higher power insets of panels (c) and (d) illustrate patches of fibronectin immunoreactivity within capillaries, with more intense fibronectin immunolabelling present within AD tissue. White arrows illustrate an absence of fibronectin immunoreactivity, black arrows illustrate the presence of fibronectin immunoreactivity. Significance values for a-b are based on p-values from a two-tailed unpaired t-test with Welch's correction for unequal variance. *p < 0.05, **p < 0.01. Scale bar corresponds to 100 μm in c-d, 50 μm for e-f. Ctrl = control; AD = Alzheimer's disease; Gra = granule cell layer; Mol = molecular cell layer; Fibro = fibronectin.

et al., 2017). We quantified IBA1 immunoreactivity and reported a significant increase in IBA1 expression and coverage within AD neocerebellar TMA cores. Investigation of IBA1 in whole neocerebellar sections demonstrated no differences in the number of IBA1-positive cells between control and AD cases. However, normalisation of IBA1 integrated intensity to cell number still demonstrated a significant increase in IBA1 expression per cell in AD cases. These data suggest that the increase in IBA1 expression is an indicator of a potential microglial reactive response (Ito et al., 1998; Ito et al., 2001), occurring in the AD neocerebellum without any overt change in the absolute number of microglia (Hopperton et al., 2017). We investigated IBA1 cellular morphology and reported a significant reduction in IBA1-positive microglial process length and number of branches within the AD neocerebellum, which further supports the hypothesis that phenotypic change within existing IBA1 microglia, rather than proliferation, contributes towards the glial responses within the human brain (Serrano-Pozo et al., 2013).

Human leukocyte antigen D-related (HLA-DR) is a type of major histocompatibility complex II (MHCII) expressed on the surface of antigen-presenting cells and is widely responsible for antigen presentation and adaptive immune system activation. HLA-DR is generally

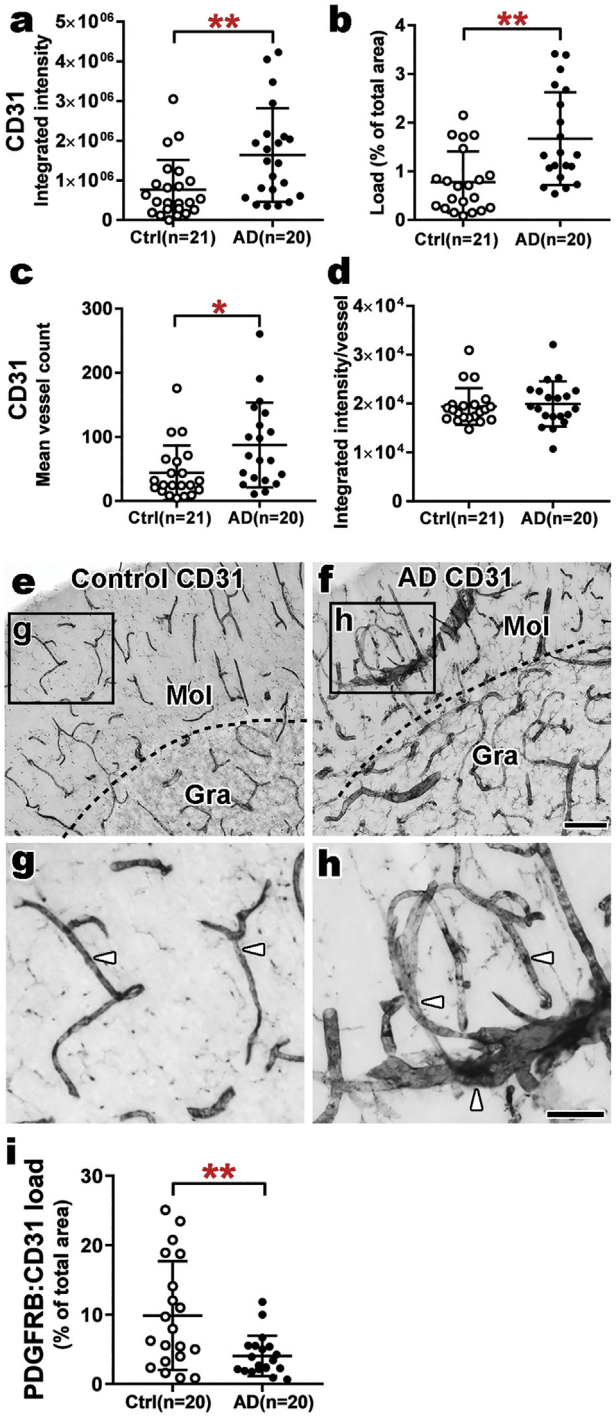

Fig. 7. Increase in CD31-positive vessels in AD neocerebellum tissue. CD31 levels were found to be significantly elevated in AD ($n = 20$) compared to control (n = 21) cases in TMA 15, evidenced by (a) a 114% increase in CD31 integrated intensity ($p = 0.006$) and (b) 115% increase in CD31 load ($p = 0.001$). (c) Quantification of CD31-positive vessel number revealed a significant 98% increase in the number of vessels ($p = 0.02$) in AD cases compared to controls. (d) Integrated intensity per CD31-positive vessel was unchanged between the control and AD groups (ns; $p = 0.69$), suggesting no overall differences in CD31-positive protein expression levels in AD. (e-f) Representative photomicrographs of CD31 immunoreactivity in free-floating neocerebellar sections from (e) control case H119 and (f) AD case AZ64 illustrate an increase in the number of CD31-positive vessels in AD. (g-h) Higher power insets of panels (e) and (f) illustrate a greater number of CD31-positive vessels in the AD neocerebellum. White arrows illustrate CD31-positive vessels. (i) The ratio of PDGFRβ:CD31 load was found to be significantly reduced by 59% ($p = 0.005$) in AD (n = 20) compared to control (n = 20) cases. Significance values for a-d are based on p-values from a two-tailed unpaired t-test with Welch's correction for unequal variance. *p < 0.05, **p < 0.01. Scale bar corresponds to 100 μm in e-f, and 50 μm for g-h. Ctrl = control; AD = Alzheimer's disease; Gra = granule cell layer; Mol = molecular cell layer; CD31 = cluster of differentiation 31.

considered a marker of activated microglial cells, though it may have weaker expression in resting microglia(McGeer et al., 1987; Lee et al., 2002). To date, of the five studies that have quantified HLA-DR immunoreactivity in the cerebellum (either protein expression or cell counts), four studies have found no differences between AD and control cases (Giulian et al., 1995; Lue et al., 2001; Van Everbroeck et al., 2004; Overmyer et al., 1999). The only study to report a difference was a semi-quantitative pilot study of HLA-DR immunoreactivity in $n = 3$ control versus n = 3 AD cases (Hensley et al., 1995). Therefore, our neocerebellar TMA data demonstrating no statistical difference in HLA-DR expression and coverage between control and AD samples is in general agreement with the majority of current studies examining HLA-DR immunoreactivity in the cerebellum. Furthermore, we conducted HLA-DR microglia cell counts in whole neocerebellar sections and found no changes in cell number between control and AD cases. Interestingly, we identified a significant reduction in both HLA-DR cellular process length and number of branches within AD cases, which reinforces the morphological and phenotypic changes underlying the HLA-DR glial response to AD within the neocerebellum. The lack of HLA-DR upregulation or changes in cell number in the AD neocerebellum, combined with the presence of considerable dendritic morphology changes is consistent with the viewpoint that microglial changes in AD are widely due to a phenotypic change of resting microglial cells, rather than the prospect of any proliferation (Serrano-Pozo et al., 2013).

4.3. Absence of astrocytosis in the AD neocerebellum

Glial fibrillary acidic protein (GFAP) is a class III intermediate filament protein generally used as a marker of reactive astrocytosis in pathological conditions (Garwood et al., 2017; Sofroniew and Vinters, 2010). We investigated if reactive astrocytosis was present in the neocerebellum in AD through quantification of GFAP immunoreactivity. Our results demonstrated no differences in GFAP expression or coverage between control and AD cases, which suggests an absence of reactive astrocytosis in the AD neocerebellum. Our results corroborate an immunohistochemical study of 12 AD and 12 control human brains, which assessed another astrocytic protein also considered a marker of astrocytic activation, S100 calcium-binding protein β (S100β), reporting no changes in the AD cerebellum despite extensive upregulation in cortical regions in AD (Van Eldik and Griffin, 1994). Furthermore, our results also corroborate a densitometric study of GFAP-positive astrocytes in 10 sporadic AD cases and 10 controls, which reported no differences in the density of GFAP-positive astrocytes in the cerebellar granule layer of the AD cases compared to the control cohort (Fukutani et al., 1996). The absence of astrocytosis within the AD neocerebellum may be attributable to a lack of cerebellar neurofibrillary tangles (NFTs) present within the tissue. Studies assessing gliosis within the AD cerebral cortex suggest that an increase in the number of astrocytes parallels an increase in the number of NFTs, while the number of GFAP astrocytes have been shown to correlate with the Braak stage of NFTs (Serrano-Pozo et al., 2011; Simpson et al., 2010). Thus, the lack of GFAP upregulation and NFTs in the AD neocerebellum reinforces the potential pathological relationship between astrocytosis and tau pathology, which can be inferred from human neocortical AD studies (Simpson et al., 2010; Serrano-Pozo et al., 2011; Serrano-Pozo et al., 2013).

4.4. Increased expression of basement membrane-associated ECM molecules in AD neocerebellum

Currently, there are no studies available which have quantified various components of basement membrane-associated extracellular matrix (ECM) molecules such as collagen IV, or fibronectin within AD neocerebellar samples compared to control brains. Therefore we decided to investigate these molecules within the AD neocerebellum.

Although collagen IV and fibronectin are both proteins secreted by endothelial cells, astrocytes and pericytes found in the periphery and vasculature of the brain, greater fibronectin deposition in the AD neocerebellum with no overt change in collagen IV may be related to differences in the roles of both proteins in the brain. Collagen IV is a structural protein involved in stabilizing and providing strength to the basement-membrane through interacting with other proteins including laminin, nidogen and perlecan (Brachvogel and Mayer, 2004). Our data suggests that collagen IV is not excessively deposited within the AD neocerebellum, compared to the neocortex, where studies have documented increases in cortical vascular collagen IV (Kalaria and Pax, 1995; Farkas et al., 2000; Lepelletier et al., 2017).

In contrast to collagen IV, our study demonstrated a significant increase in vascular fibronectin expression within the neocerebellar vasculature using the TMA approach and whole section validation. These results corroborate recent reports of increased fibronectin immunoreactivity within the neocortex (Lepelletier et al., 2017) and previous reports of increased fibronectin within plasma of AD patients (Lemańska-Perek et al., 2009; Muenchhoff et al., 2014). Fibronectin is a specialized protein involved in several cellular processes including adhesion, migration, proliferation, transformation, matrix remodeling, tissue repair, wound healing and hemostasis (Mao and Schwarzbauer, 2005; Geiger et al., 2001). Fibronectin also demonstrates a strong angiogenic influence and promotion of survival and proliferation of brain endothelial cells (Wang and Milner, 2006; Milner, 2007). Therefore, the increase in fibronectin and its established role in endothelial cell survival, proliferation and adhesion is in agreement with our reported increase in blood-vessels immunopositive for human platelet endothelial cell adhesion molecule (CD31), which we discuss in the context of potential angiogenesis/hypervascularisation below.

4.5. Neurovascular changes in the AD neocerebellum

Our study is the first to report a quantitative increase in the number of CD31/PECAM-1-positive blood vessels within the AD neocerebellum through TMA analysis. Human platelet endothelial cell adhesion molecule (CD31/PECAM-1) is a transmembrane protein known to be highly expressed by endothelial cells (localised to intercellular junctions), in addition to leukocytes and platelets which in turn are known to be involved in the deposition of amyloid-β and inflammation (Casoli et al., 2010; Gianfranco and Elisabetta, 2004). Previous studies have shown elevated CD31 levels within the plasma of AD patients compared to controls (Casoli et al., 2010; Nielsen et al., 2007; Xue et al., 2012). Therefore, we investigated CD31 expression, coverage and number of immunopositive blood vessels within the neocerebellum. Although we initially found an increase in the expression and coverage of CD31 in the AD neocerebellum, these findings were not significant when vessel number was taken into account within the control and AD cohorts, thereby suggesting these changes in expression/coverage are widely attributable to an increase in the number of CD31-positive blood vessels. These results could be an indication of possible angiogenic processes occurring within the neocerebellum as reported in other areas of the human AD brain, including possible hypervascularisation and increased expression of angiogenic factors which warrants further investigation (Buee et al., 1992; Biron et al., 2011; Tarkowski et al., 2002). Furthermore, whether this increase in the number of CD31-positive blood vessels in the AD neocerebellum is due to an increase in the absolute number of endothelial cells, or other factors which may impact vascular density (such as tissue volume), requires future investigation with high-resolution and design-based stereological techniques.

We also investigated mural cell markers platelet-derived growth factor receptor beta (PDGFRβ) and alpha smooth muscle actin (αSMA) in the AD neocerebellum. We quantified the expression and coverage of PDGFRβ, a marker for capillary-associated pericytes, and α-SMA, a marker for vascular smooth muscle cells around large vessels using the TMA approach. Our data demonstrates that the expression and coverage of PDGFRβ and α-SMA lining the neurovasculature are not altered in the neocerebellum in AD, suggesting wider preservation of neocerebellar vascular mural cells in AD. However, we show for the first time, a reduction in PDGFRβ:CD31 load within the AD neocerebellum, which may suggest that hypervascularisation could be accompanied by failure to invest perivascular cells (Bell et al., 2010). There is an emerging body of evidence in both AD animal models and patient neuroimaging studies which suggest that neovascular changes in AD occur before cognitive decline, amyloid-β deposition and neuropathology (Iadecola et al., 1999; Knopman and Roberts, 2010; Ruitenberg et al., 2005; Zlokovic, 2011). Thus, our data supports the notion that neovascular disruption, notably changes affecting basement membrane-associated ECM molecules and endothelial cells, may be a dissociated event from AD neuropathology, as suggested by the scant AD pathology within the neocerebellum in the presence of significant neovascular changes.

4.6. Methodological considerations

As with any neuropathological study utilising post-mortem human tissue, there is variability from case to case, or region to region, despite analogous post-mortem processing procedures, which reflects the natural variation associated with studying human subjects (Ferrer et al., 2008). This variation has been particularly vital in understanding the cellular basis for symptom heterogeneity in other neurodegenerative disorders studied in our laboratory, such as Huntington's disease (Singh-Bains et al., 2019). One of the variables which cannot be controlled in human neuropathological studies is the primary cause of death for the cases. In the TMA, the most common cause of death for the AD cases were respiratory-related complications including pneumonia (Table 2). In comparison, the most common cause of death for neurologically normal control brains were cardiac-related complications (Table 1). We have published many papers in human Alzheimer's disease and Huntington's disease where these differences are apparent in the case cohorts (Narayan et al., 2015b; Coppieters et al., 2014; Singh-Bains et al., 2019; Mehrabi et al., 2016). Many studies have reported pneumonia as the most common physiological cause of death for AD patients, and is widely attributable to dysphagia causing the ingestion of food into the respiratory system, leading to aspiration pneumonia (Todd et al., 2013; Kukull et al., 1994; Bosch et al., 2012). Pneumonia causes significantly more deaths in AD patients than the general population and is a frequent complication in patients with advanced dementia (Todd et al., 2013). In comparison, ischemic heart disease is the leading cause of death for the general population, including patients without a neurological disease (Bloomfield, 2017). Therefore, while it is to be acknowledged that the differences in cause of death between the control and AD cohorts may be considered a confounding variable in this study, it can also be argued that pneumonia is in fact a clinical consequence of end-stage AD pathology.

While we matched demographic variables including post-mortem delay and age at death between the control and AD cohorts, we were unable to sex-match cases in this study. Therefore, we conducted additional analyses to investigate the impact of sex differences on the altered microglia and neurovasculature in the AD neocerebellum (Additional file 2: Supplementary Fig. 2a-f). We compared our IBA1, fibronectin and CD31 expression data between males in females from the pooled TMA data, and separately between the control and AD cohorts. We can conclude that gender has no impact on our reported

microglial and vascular changes in the neocerebellum in AD.

Additionally, a future direction would be to understand the possible underlying genetic basis for the altered microglia and neurovasculature in the AD neocerebellum, because of the relevance of the Apolipoprotein E (APOE) genotype for the severity of AD pathology (Iacono et al., 2009; Serrano-Pozo et al., 2013). A previous study which quantified the absolute numbers of IBA1 positive microglia in a section of human temporal cortex demonstrated that the number of IBA1 positive microglia did not differ between APOE ε4 carriers and non-carriers (Serrano-Pozo et al., 2013). However, APOE ε4 carriers had a greater number of IBA1-HLADR positive colabeled cells, which could serve as an exciting avenue to pursue in the future using immunohistochemical co-labelling techniques in the neocerebellum. Unfortunately, the Human Brain Bank clinicodemographic information does not include the APOE genetic status of the cases used for the TMA studies. Furthermore, the formalin-fixed paraffin embedded blocks used for the construction of the TMA is optimally processed for immunohistochemistry, and not DNA extraction for genetic studies due to formalin concentration and storage times (Srinivasan et al., 2002). Therefore, using tissue preservation methods optimized for genomic studies, investigating the impact of the APOE status on microglia and neurovasculature could be an exciting avenue for the future.

5. Conclusions

In conclusion, this is the first study of its kind to undertake a tissue microarray screening approach as a means to investigate the human neocerebellum in AD. We demonstrate that this approach recapitulates subtle features of neocerebellar AD pathology, including the upregulation of neocerebellar amyloid-β, with no significant changes in tau, ubiquitin, or Purkinje cell number. The lack of neuronal degeneration provided a context to extend our investigation to non-neuronal cells, in order to identify more subtle AD-related molecular changes which would be difficult to detect in more severely degenerated regions. Our investigation of IBA1- and HLA-DR-positive microglia revealed morphological and protein expression changes, with no changes in cellular numbers, reinforcing that microglia do not proliferate in AD, but assume an altered phenotype. We also reported significant basement membrane-associated extracellular matrix molecular changes and neurovascular changes, as evidenced by increased expression of fibronectin with a greater number of CD31-positive vessels in a region of the AD brain traditionally considered to be devoid of major neuropathology. Taken together, these data support the notion that microglial and vascular changes are vital components of disease progression within the neocerebellum. The significant neurovascular and microglial changes occurring without major features of traditional AD neuropathology suggest that these changes occur early in cerebellar AD pathogenesis, independent of neuronal loss and tau-tangle formation. Future studies are needed to determine if these changes are causative, contributing, or a consequence of the disease, which warrants further investigation. Therefore, we conclude the neocerebellum is not a silent bystander in AD, based on our evidence that AD-related molecular changes occur within non-neuronal cells, supporting the hypothesis that there is a cerebellar role in the pathogenesis of AD.

Supplementary data to this article can be found online at https://doi.org/10.1016/j.nbd.2019.104589.

Ethics approval and consent to participate

Studies undertaken using these tissues were approved by the Northern Regional Ethics Committee (New Zealand) and informed consent was obtained from all donors. All methods were carried out in accordance with the approved guidelines.

Consent for publication

Not applicable as this manuscript does not contain individual/personal details of subjects.

Availability of data and material

The data presented in this study are included in the manuscript and Additional files. Additional data that are not included can be made available upon reasonable request to the corresponding author.

Declaration of Competing Interests

The authors declare that they have no competing interests.

Funding

This work was supported by the Health Research Council of New Zealand (11-802), Brain Research New Zealand, Neurological Foundation of New Zealand (1102-PG), Hugh Green Foundation, The Coker Trust, the Sir Thomas and Lady Duncan Trust and by the Freemasons Foundation of New Zealand through a postdoctoral research fellowship to MKSB.

Authors' contributions

MKSB contributed to study design, data acquisition and analysis, and production of manuscript and figures VL, MDRA, AYST, NFM and ELS contributed to data acquisition and analysis. RLMF and MD contributed to study concept, design and production of manuscript and figures. All authors have read and approved the final manuscript.

Acknowledgements

We express our appreciation to all donor families in New Zealand, who through their generosity have enabled this study to be undertaken through their invaluable tissue donation to the New Zealand Neurological Foundation Human Brain Bank. We thank Dr. Beth Synek and Dr. Clinton Turner for their expert neuropathological assessments of the cases in this study. We acknowledge the excellent work and assistance of Marika Eszes (Human Brain Bank) and Kristina Hubbard (Research Technician). We acknowledge the staff at the Biomedical Imaging Research Unit (Ratish Kurian) for V-slide Scanner support. This work was supported by a Programme Grant from the Health Research Council of New Zealand, Brain Research New Zealand, Neurological Foundation of New Zealand, Hugh Green Foundation, The Coker Trust, the Sir Thomas and Lady Duncan Trust and by the Freemasons Foundation of New Zealand.

References

Adams, S.L., Tilton, K., Kozubek, J.A., Seshadri, S., Delalle, I., 2016. Subcellular changes in bridging integrator 1 protein expression in the cerebral cortex during the progression of Alzheimer disease pathology. J. Neuropathol. Exp. Neurol. 75, 779–790.

Albus, J.S., 1971. A theory of cerebellar function. Math. Biosci. 10, 25–61.

Andersen, K., Andersen, B.B., Pakkenberg, B., 2012. Stereological quantification of the cerebellum in patients with Alzheimer's disease. Neurobiol. Aging 33 197. e11-197. e20.

Bas, O., Acer, N., Mas, N., Karabekir, H.S., Kusbeci, O.Y., Sahin, B., 2009. Stereological evaluation of the volume and volume fraction of intracranial structures in magnetic resonance images of patients with Alzheimer's disease. Ann. Anatom. Anatomischer Anzeiger 191, 186–195.

Baumann, O., Borra, R.J., Bower, J.M., Cullen, K.E., Habas, C., Ivry, R.B., Leggio, M., Mattingley, J.B., Molinari, M., Moulton, E.A., 2015. Consensus paper: the role of the cerebellum in perceptual processes. Cerebellum 14, 197–220.

Bell, R.D., Zlokovic, B.V., 2009. Neurovascular mechanisms and blood–brain barrier disorder in Alzheimer's disease. Acta Neuropathol. 118, 103–113.

Bell, R.D., Winkler, E.A., Sagare, A.P., Singh, I., Larue, B., Deane, R., Zlokovic, B.V., 2010. Pericytes control key neurovascular functions and neuronal phenotype in the adult brain and during brain aging. Neuron 68, 409–427.

Biron, K.E., Dickstein, D.L., Gopaul, R., Jefferies, W.A., 2011. Amyloid triggers extensive cerebral angiogenesis causing blood brain barrier permeability and hypervascularity in Alzheimer's disease. PLoS One 6, e23789.
Bloomfield, A., 2017. Health and Independence Report 2017. The Director-General of Health's Annual Report on the State of Public Health. Ministry of Health, Wellington, New Zealand.
Bosch, X., Formiga, F., Cuerpo, S., Torres, B., Rosón, B., López-Soto, A., 2012. Aspiration pneumonia in old patients with dementia. Prognostic factors of mortality. Eur. J. Internal Med. 23, 720–726.
Braak, H., Braak, E., 1991. Neuropathological stageing of Alzheimer-related changes. Acta Neuropathol. 82, 239–259.
Braak, H., Braak, E., 1995. Staging of alzheimer's disease-related neurofibrillary changes. Neurobiol. Aging 16, 271–278.
Braak, H., Braak, E., 1997a. Diagnostic criteria for neuropathologic assessment of Alzheimer's disease. Neurobiol. Aging 18, S85–S88.
Braak, H., Braak, E., 1997b. Frequency of stages of Alzheimer-related lesions in different age categories. Neurobiol. Aging 18, 351–357.
Braak, H., Braak, E., Bohl, J., Lang, W., 1989. Alzheimer's disease: amyloid plaques in the cerebellum. J. Neurol. Sci. 93, 277–287.
Brachvogel, P.E.S.-S.U., Mayer, B.S.K.N.Y., 2004. U: collagen IV is essential for basement membrane stability but dispensable for initiation of its assembly during early development. Development 131, 1619–1628.
Buckner, R.L., Krienen, F.M., Castellanos, A., Diaz, J.C., Yeo, B.T., 2011. The organization of the human cerebellum estimated by intrinsic functional connectivity. J. Neurophysiol. 106, 2322–2345.
Buee, L., Hof, P.R., Roberts, D.D., Delacourte, A., Morrison, J.H., Fillit, H.M., 1992. Immunohistochemical identification of thrombospondin in normal human brain and in Alzheimer's disease. Am. J. Pathol. 141, 783–788.
Canu, E., Mclaren, D.G., Fitzgerald, M.E., Bendlin, B.B., Zoccatelli, G., Alessandrini, F., Pizzini, F.B., Ricciardi, G.K., Beltramello, A., Johnson, S.C., 2010. Microstructural diffusion changes are independent of macrostructural volume loss in moderate to severe Alzheimer's disease. J. Alzheimers Dis. 19, 963–976.
Casoli, T., Di Stefano, G., Balietti, M., Solazzi, M., Giorgetti, B., Fattoretti, P., 2010. Peripheral inflammatory biomarkers of Alzheimer's disease: the role of platelets. Biogerontology 11, 627–633.
Cisbani, G., Freeman, T.B., Soulet, D., Saint-Pierre, M., Gagnon, D., Parent, M., Hauser, R.A., Barker, R.A., Cicchetti, F., 2013. Striatal allografts in patients with Huntington's disease: impact of diminished astrocytes and vascularization on graft viability. Brain 136, 433–443.
Coppieters, N., Dieriks, B.V., Lill, C., Faull, R.L.M., Curtis, M.A., Dragunow, M., 2014. Global changes in DNA methylation and hydroxymethylation in Alzheimer's disease human brain. Neurobiol. Aging 35, 1334–1344.
Dickson, D.W., Wertkin, A., Mattiace, L.A., Fier, E., Kress, Y., Davies, P., Yen, S.H., 1990. Ubiquitin immunoelectron microscopy of dystrophic neurites in cerebellar senile plaques of Alzheimer's disease. Acta Neuropathol. 79, 486–493.
Dieriks, B.V., Park, T.I., Fourie, C., Faull, R.L., Dragunow, M., Curtis, M.A., 2017. Alpha-synuclein transfer through tunneling nanotubes occurs in SH-SY5Y cells and primary brain pericytes from Parkinson's disease patients. Sci. Rep. 7, 42984.
Dragunow, M., Feng, S., Rustenhoven, J., Curtis, M., Faull, R., 2016. Studying human brain inflammation in leptomeningeal and choroid plexus explant cultures. Neurochem. Res. 41, 579–588.
Dukart, J., Mueller, K., Horstmann, A., Vogt, B., Frisch, S., Barthel, H., Becker, G., Möller, H.E., Villringer, A., Sabri, O., 2010. Differential effects of global and cerebellar normalization on detection and differentiation of dementia in FDG-PET studies. Neuroimage 49, 1490–1495.
Farkas, E., De Jong, G.I., Vos, De, R. a. I., Jansen Steur, E. N. H. & Luiten, P. G. M., 2000. Pathological features of cerebral cortical capillaries are doubled in Alzheimer's disease and Parkinson's disease. Acta Neuropathol. 100, 395–402.
Ferrer, I., Martinez, A., Boluda, S., Parchi, P., Barrachina, M., 2008. Brain banks: benefits, limitations and cautions concerning the use of post-mortem brain tissue for molecular studies. Cell Tissue Bank. 9, 181.
Fukutani, Y., Cairns, N.J., Rossor, M.N., Lantos, P.L., 1996. Purkinje cell loss and astrocytosis in the cerebellum in familial and sporadic Alzheimer's disease. Neurosci. Lett. 214, 33–36.
Fukutani, Y., Cairns, N.J., Rossor, M.N., Lantos, P.L., 1997. Cerebellar pathology in sporadic and familial Alzheimer's disease including APP 717 (Val→ Ile) mutation cases: a morphometric investigation. J. Neurol. Sci. 149, 177–184.
Furukawa, Y., Iseki, E., Hino, H., Kanai, A., Odawara, T., Kosaka, K., 2004. Ubiquitin and ubiquitin-related proteins in neurons and dendrites of brains of atypical Pick's disease without Pick bodies. Neuropathology 24, 38–45.
Garbuzova-Davis, S., Mirtyl, S., Sallot, S.A., Hernandez-Ontiveros, D.G., Haller, E., Sanberg, P.R., 2013. Blood-brain barrier impairment in MPS III patients. BMC Neurol. 13, 174.
Garwood, C., Ratcliffe, L., Simpson, J., Heath, P., Ince, P., Wharton, S., 2017. Astrocytes in Alzheimer's disease and other age-associated dementias: a supporting player with a central role. Neuropathol. Appl. Neurobiol. 43, 281–298.
Geiger, B., Bershadsky, A., Pankov, R., Yamada, K.M., 2001. Transmembrane crosstalk between the extracellular matrix and the cytoskeleton. Nat. Rev. Mol. Cell Biol. 2, 793.
Gianfranco, B., Elisabetta, D., 2004. Endothelial cell-to-cell junctions: molecular organization and role in vascular homeostasis. Physiol. Rev. 84, 869–901.
Giulian, D., Haverkamp, L.J., Li, J., Karshin, W.L., Yu, J., Tom, D., Li, X., Kirkpatrick, J.B., 1995. Senile plaques stimulate microglia to release a neurotoxin found in Alzheimer brain. Neurochem. Int. 27, 119–137.
Gottardi, C.J., Wilcox, D.R., Van Roy, F., Van Hengel, J., Tyberghein, K., De Bleser, P., Folmsbee, S.S., Tourtellotte, W.G., 2016. αT-catenin in restricted brain cell types and its potential connection to autism. J. Mol. Psychiatr. 4, 2.
Guo, C.C., Tan, R., Hodges, J.R., Hu, X., Sami, S., Hornberger, M., 2016. Network-selective vulnerability of the human cerebellum to Alzheimer's disease and frontotemporal dementia. Brain 139, 1527–1538.
Habas, C., Kamdar, N., Nguyen, D., Prater, K., Beckmann, C.F., Menon, V., Greicius, M.D., 2009. Distinct cerebellar contributions to intrinsic connectivity networks. J. Neurosci. 29, 8586–8594.
Haider, L., Fischer, M.T., Frischer, J.M., Bauer, J., Höftberger, R., Botond, G., Esterbauer, H., Binder, C.J., Witztum, J.L., Lassmann, H., 2011. Oxidative damage in multiple sclerosis lesions. Brain 134, 1914–1924.
Haines, D.E., Dietrichs, E., 1984. An HRP study of hypothalamo-cerebellar and cerebello-hypothalamic connections in squirrel monkey (saimiri sciureus). J. Comp. Neurol. 229, 559–575.
Haines, D.E., Dietrichs, E., Mihailoff, G.A., Mcdonald, E.F., 1997. The cerebellar-hypothalamic axis: basic circuits and clinical observations. In: International Review of Neurobiology. Elsevier.
Hensley, K., Hall, N., Subramaniam, R., Cole, P., Harris, M., Aksenov, M., Aksenova, M., Gabbita, S.P., Wu, J.F., Carney, J.M., 1995. Brain regional correspondence between Alzheimer's disease histopathology and biomarkers of protein oxidation. J. Neurochem. 65, 2146–2156.
Heppner, F.L., Ransohoff, R.M., Becher, B., 2015. Immune attack: the role of inflammation in Alzheimer disease. Nat. Rev. Neurosci. 16, 358.
Hopperton, K.E., Mohammad, D., Trépanier, M.O., Giuliano, V., Bazinet, R.P., 2017. Markers of microglia in post-mortem brain samples from patients with Alzheimer's disease: a systematic review. Mol. Psychiatry 23 (2), 177–198.
Iacono, D., Markesbery, W.R., Gross, M., Pletnikova, O., Rudow, G., Zandi, P., Troncoso, J.C., 2009. The Nun study: clinically silent AD, neuronal hypertrophy, and linguistic skills in early life. Neurology 73, 665–673.
Iadecola, C., Zhang, F., Niwa, K., Eckman, C., Turner, S.K., Fischer, E., Younkin, S., Borchelt, D.R., Hsiao, K.K., Carlson, G.A., 1999. SOD1 rescues cerebral endothelial dysfunction in mice overexpressing amyloid precursor protein. Nat. Neurosci. 2, 157.
Ihara, Y., Morishima-Kawashima, M., Nixon, R., 2012. The ubiquitin–proteasome system and the autophagic–lysosomal system in Alzheimer disease. Cold Spring Harb. Perspect. Med. 2, a006361.
Imai, Y., Ibata, I., Ito, D., Ohsawa, K., Kohsaka, S., 1996. A novel geneiba1in the major histocompatibility complex class III region encoding an EF hand protein expressed in a monocytic lineage. Biochem. Biophys. Res. Commun. 224, 855–862.
Ito, D., Imai, Y., Ohsawa, K., Nakajima, K., Fukuuchi, Y., Kohsaka, S., 1998. Microglia-specific localisation of a novel calcium binding protein, Iba1. Mol. Brain Res. 57, 1–9.
Ito, D., Tanaka, K., Suzuki, S., Dembo, T., Fukuuchi, Y., 2001. Enhanced expression of Iba1, ionized calcium-binding adapter molecule 1, after transient focal cerebral ischemia in rat brain. Stroke 32, 1208–1215.
Jansson, D., Graham, E.S., Mee, E.W., Scotter, E.L., Rustenhoven, J., Smyth, L.C.D., Dragunow, M., Coppieters, N., Bergin, P.S., Faull, R.L.M., 2016. Interferon-γ blocks signalling through PDGFRβ in human brain pericytes. J. Neuroinflammation 13, 249.
Joachim, C.L., Morris, J.H., Selkoe, D.J., 1989. Diffuse senile plaques occur commonly in the cerebellum in Alzheimer's disease. Am. J. Pathol. 135, 309.
Kalaria, R.N., Pax, A.B., 1995. Increased collagen content of cerebral microvessels in Alzheimer's disease. Brain Res. 705, 349–352.
Keable, A., Fenna, K., Yuen, H.M., Johnston, D.A., Smyth, N.R., Smith, C., Al-Shahi Salman, R., Samarasekera, N., Nicoll, J.A., Attems, J., Kalaria, R.N., Weller, R.O., Carare, R.O., 2016. Deposition of amyloid beta in the walls of human leptomeningeal arteries in relation to perivascular drainage pathways in cerebral amyloid angiopathy. Biochim. Biophys. Acta 1862, 1037–1046.
Keller, J.N., Hanni, K.B., Markesbery, W.R., 2000. Impaired proteasome function in Alzheimer's disease. J. Neurochem. 75, 436–439.
Knopman, D.S., Roberts, R., 2010. Vascular risk factors: imaging and neuropathologic correlates. J. Alzheimers Dis. 20, 699–709.
Kukull, W.A., Brenner, D.E., Speck, C.E., Nochlin, D., Bowen, J., Mccormick, W., Teri, L., Pfanschmidt, M.L., Larson, E.B., 1994. Causes of death associated with Alzheimer disease: variation by level of cognitive impairment before death. J. Am. Geriatr. Soc. 42, 723–726.
Kurbatskaya, K., Phillips, E.C., Croft, C.L., Dentoni, G., Hughes, M.M., Wade, M.A., Al-Sarraj, S., Troakes, C., O'neill, M.J., Perez-Nievas, B.G., Hanger, D.P., Noble, W., 2016. Upregulation of calpain activity precedes tau phosphorylation and loss of synaptic proteins in Alzheimer's disease brain. Acta Neuropathol. Commun. 4, 34.
Lee, Y.B., Nagai, A., Kim, S.U., 2002. Cytokines, chemokines, and cytokine receptors in human microglia. J. Neurosci. Res. 69, 94–103.
Lemańska-Perek, A., Leszek, J., Krzyżanowska, G., B, D., Radzik, J., Ką & Tnik-Prastowska, I., 2009. Molecular status of plasma Fibronectin as an additional biomarker for assessment of Alzheimer's dementia risk. Dement. Geriatr. Cogn. Disord. 28, 338–342.
Lepelletier, F.X., Mann, D.M.A., Robinson, A.C., Pinteaux, E., Boutin, H., 2017. Early changes in extracellular matrix in Alzheimer's disease. Neuropathol. Appl. Neurobiol. 43, 167–182.
Li, Y.-T., Woodruff-Pak, D.S., Trojanowski, J.Q., 1994. Amyloid plaques in cerebellar cortex and the integrity of Purkinje cell dendrites. Neurobiol. Aging 15, 1–9.
Lowe, M.T.J., Faull, R.L.M., Christie, D.L., Waldvogel, H.J., 2015. Distribution of the creatine transporter throughout the human brain reveals a spectrum of creatine transporter immunoreactivity. J. Comp. Neurol. 523, 699–725.
Lue, L.-F., Walker, D.G., Brachova, L., Beach, T.G., Rogers, J., Schmidt, A.M., Stern, D.M., Du Yan, S., 2001. Involvement of microglial receptor for advanced glycation end-products (RAGE) in Alzheimer's disease: identification of a cellular activation mechanism. Exp. Neurol. 171, 29–45.
Mao, Y., Schwarzbauer, J.E., 2005. Fibronectin fibrillogenesis, a cell-mediated matrix assembly process. Matrix Biol. 24, 389–399.

Mcgeer, P.L., Itagaki, S., Tago, H., Mcgeer, E.G., 1987. Reactive microglia in patients with senile dementia of the Alzheimer type are positive for the histocompatibility glycoprotein HLA-DR. Neurosci. Lett. 79, 195–200.
Mehrabi, N.F., Waldvogel, H.J., Tippett, L.J., Hogg, V.M., Synek, B.J., Faull, R.L.M., 2016. Symptom heterogeneity in Huntington's disease correlates with neuronal degeneration in the cerebral cortex. Neurobiol. Dis. 96, 67–74.
Milner, R., 2007. A novel three-dimensional system to study interactions between endothelial cells and neural cells of the developing central nervous system. BMC Neurosci. 8, 3.
Mirra, S.S., Heyman, A., Mckeel, D., Sumi, S.M., Crain, B.J., Brownlee, L.M., Vogel, F.S., Hughes, J.P., Van Belle, G., Berg, L., Ball, M.J., Bierer, L.M., Claasen, D., Hansen, L.R., Hart, M., Hedreen, J., Baltimore, B., Hen Derson, V., Hyman, B.T., Joachim, C., Mark-Esbery, W., Mar Tinez, A.J., Mckee, A., Miller, C., Moossy, J., Nochlin, D., Perl, D., Petito, C., Rao, G.R., Schelper, R.L., Slager, U., Terry, R.D., 1991. The consortium to establish a registry for Alzheimer's disease (CERAD). Part II. Standardization of the neuropathologic assessment of Alzheimer's disease. Neurology 41, 479–486.
Montine, T.J., Monsell, S.E., Beach, T.G., Bigio, E.H., Bu, Y., Cairns, N.J., Frosch, M., Henriksen, J., Kofler, J., Kukull, W.A., 2016. Multisite assessment of NIA-AA guidelines for the neuropathologic evaluation of Alzheimer's disease. Alzheimers Dement. 12, 164–169.
Moore, G.R., Laule, C., Leung, E., Pavlova, V., Morgan, B.P., Esiri, M.M., 2016. Complement and humoral adaptive immunity in the human choroid plexus: roles for stromal concretions, basement membranes, and epithelium. J. Neuropathol. Exp. Neurol. 75, 415–428.
Muenchhoff, J., Poljak, A., Song, F., Raftery, M., Brodaty, H., Duncan, M., Mcevoy, M., Attia, J., Schofield, P.W., Sachdev, P.S., 2014. Plasma protein profiling of mild cognitive impairment and Alzheimers disease across two independent cohorts. J. Alzheimer Dis. 43, 1355–1373.
Nakayama, D., Matsuyama, T., Ishibashi-Ueda, H., Nakagomi, T., Kasahara, Y., Hirose, H., Kikuchi-Taura, A., Stern, D.M., Mori, H., Taguchi, A., 2010. Injury-induced neural stem/progenitor cells in post-stroke human cerebral cortex. Eur. J. Neurosci. 31, 90–98.
Narayan, P.J., Dragunow, M., 2010. High content analysis of histone acetylation in human cells and tissues. J. Neurosci. Methods 193, 54–61.
Narayan, P.J., Kim, S.-L., Lill, C., Feng, S., Faull, R.L.M., Curtis, M.A., Dragunow, M., 2015a. Assessing fibrinogen extravasation into Alzheimer's disease brain using high-content screening of brain tissue microarrays. J. Neurosci. Methods 247, 41–49.
Narayan, P.J., Lill, C., Faull, R., Curtis, M.A., Dragunow, M., 2015b. Increased acetyl and total histone levels in post-mortem Alzheimer's disease brain. Neurobiol. Dis. 74, 281–294.
Neumann, M., Sampathu, D.M., Kwong, L.K., Truax, A.C., Micsenyi, M.C., Chou, T.T., Bruce, J., Schuck, T., Grossman, M., Clark, C.M., 2006. Ubiquitinated TDP-43 in frontotemporal lobar degeneration and amyotrophic lateral sclerosis. Science 314, 130–133.
Nielsen, H.M., Londos, E., Minthon, L., Janciauskiene, S.M., 2007. Soluble adhesion molecules and angiotensin-converting enzyme in dementia. Neurobiol. Dis. 26, 27–35.
Ohsawa, K., Imai, Y., Kanazawa, H., Sasaki, Y., Kohsaka, S., 2000. Involvement of Iba1 in membrane ruffling and phagocytosis of macrophages/microglia. J. Cell Sci. 113, 3073–3084.
Overmyer, M., Helisalmi, S., Soininen, H., Laakso, M., Riekkinen Sr., P., Alafuzoff, I., 1999. Reactive microglia in aging and dementia: an immunohistochemical study of postmortem human brain tissue. Acta Neuropathol. 97, 383–392.
Ruitenberg, A., Den Heijer, T., Bakker, S.L., Van Swieten, J.C., Koudstaal, P.J., Hofman, A., Breteler, M.M., 2005. Cerebral hypoperfusion and clinical onset of dementia: the Rotterdam study. Ann. Neurol. 57, 789–794.
Rustenhoven, J., Scotter, E.L., Jansson, D., Kho, D.T., Oldfield, R.L., Bergin, P.S., Mee, E.W., Faull, R.L.M., Curtis, M.A., Graham, S.E., 2015. An anti-inflammatory role for C/EBPδ in human brain pericytes. Sci. Rep. 5, 12132.
Sasaki, Y., Ohsawa, K., Kanazawa, H., Kohsaka, S., Imai, Y., 2001. Iba1 is an actin-cross-linking protein in macrophages/microglia. Biochem. Biophys. Res. Commun. 286, 292–297.
Schmahmann, J.D., 2004. Disorders of the cerebellum: ataxia, dysmetria of thought, and the cerebellar cognitive affective syndrome. J. Neuropsychiatr. Clin. Neurosci. 16, 367–378.
Schmahmann, J.D., 2016. Cerebellum in Alzheimer's disease and frontotemporal dementia: not a silent bystander. Brain 139, 1314–1318.
Schmahmann, J.D., Sherman, J.C., 1998. The cerebellar cognitive affective syndrome. Brain J. Neurol. 121, 561–579.
Schmahmann, J.D., Anderson, C.M., Newton, N., Ellis, R.D., 2001. The function of the cerebellum in cognition, affect and consciousness: empirical support for the embodied mind. Consciousness Emotion 2, 273–309.
Serrano-Pozo, A., Mielke, M.L., Gómez-Isla, T., Betensky, R.A., Growdon, J.H., Frosch, M.P., Hyman, B.T., 2011. Reactive glia not only associates with plaques but also parallels tangles in Alzheimer's disease. Am. J. Pathol. 179, 1373–1384.
Serrano-Pozo, A., Gómez-Isla, T., Growdon, J.H., Frosch, M.P., Hyman, B.T., 2013. A phenotypic change but not proliferation underlies glial responses in Alzheimer disease. Am. J. Pathol. 182, 2332–2344.
Simpson, J., Ince, P., Lace, G., Forster, G., Shaw, P., Matthews, F., Savva, G., Brayne, C., Wharton, S., 2010. Astrocyte phenotype in relation to Alzheimer-type pathology in the ageing brain. Neurobiol. Aging 31, 578–590.
Singh-Bains, M.K., Mehrabi, N.F., Sehji, T., Austria, M.D., Tan, A.Y., Tippett, L.J., Dragunow, M., Waldvogel, H.J., Faull, R.L., 2019. Cerebellar degeneration correlates with motor symptoms in Huntington disease. Ann. Neurol. 85, 396–405.
Siwek, D.F., Pandya, D.N., 1991. Prefrontal projections to the mediodorsal nucleus of the thalamus in the rhesus monkey. J. Comp. Neurol. 312, 509–524.
Sjöbeck, M., Englund, E., 2001. Alzheimer's disease and the cerebellum: a morphologic study on neuronal and glial changes. Dement. Geriatr. Cogn. Disord. 12, 211–218.
Smith, M.A., Harris, P.L.R., Sayre, L.M., Beckman, J.S., Perry, G., 1997. Widespread peroxynitrite-mediated damage in Alzheimer's disease. J. Neurosci. 17, 2653–2657.
Smith, A.M., Gibbons, H.M., Oldfield, R.L., Bergin, P.M., Mee, E.W., Faull, R.L.M., Dragunow, M., 2013. The transcription factor PU. 1 is critical for viability and function of human brain microglia. Glia 61, 929–942.
Sofroniew, M.V., Vinters, H.V., 2010. Astrocytes: biology and pathology. Acta Neuropathol. 119, 7–35.
Spillantini, M.G., Crowther, R.A., Jakes, R., Hasegawa, M., Goedert, M., 1998. α-Synuclein in filamentous inclusions of Lewy bodies from Parkinson's disease and dementia with Lewy bodies. Proc. Natl. Acad. Sci. 95, 6469–6473.
Srinivasan, M., Sedmak, D., Jewell, S., 2002. Effect of fixatives and tissue processing on the content and integrity of nucleic acids. Am. J. Pathol. 161, 1961–1971.
Stępień, T., Wierzba-Bobrowicz, T., Lewandowska, E., Szpak, G., 2012. Morphological and quantitative analysis of cerebellar cortical cells in Alzheimer's disease. Folia Neuropathol. 50, 250–260.
Stokum, J.A., Mehta, R.I., Ivanova, S., Yu, E., Gerzanich, V., Simard, J.M., 2015. Heterogeneity of aquaporin-4 localization and expression after focal cerebral ischemia underlies differences in white versus grey matter swelling. Acta Neuropathol. Commun. 3, 61.
Tarkowski, E., Issa, R., Sjogren, M., Wallin, A., Blennow, K., Tarkowski, A., Kumar, P., 2002. Increased intrathecal levels of the angiogenic factors VEGF and TGF-beta in Alzheimer's disease and vascular dementia. Neurobiol. Aging 23, 237–243.
Thach, W.T., 1996. On the specific role of the cerebellum in motor learning and cognition: clues from PET activation and lesion studies in man. Behav. Brain Sci. 19, 411–433.
Thal, D.R., Rüb, U., Orantes, M., Braak, H., 2002. Phases of Aβ-deposition in the human brain and its relevance for the development of AD. Neurology 58, 1791–1800.
Todd, S., Barr, S., Passmore, A.P., 2013. Cause of death in Alzheimer's disease: a cohort study. QJM 106, 747–753.
Van Eldik, L.J., Griffin, W.S.T., 1994. S100β expression in Alzheimer's disease: relation to neuropathology in brain regions. Biochimica et Biophysica Acta (BBA) 1223, 398–403.
Van Everbroeck, B., Dobbeleir, I., De Waele, M., De Leenheir, E., Lübke, U., Martin, J.-J., Cras, P., 2004. Extracellular protein deposition correlates with glial activation and oxidative stress in Creutzfeldt-Jakob and Alzheimer's disease. Acta Neuropathol. 108, 194–200.
Waldvogel, H.J., Curtis, M.A., Baer, K., Rees, M.I., Faull, R.L.M., 2007. Immunohistochemical staining of post-mortem adult human brain sections. Nat. Protoc. 1, 2719–2732.
Waldvogel, H.J., Bullock, J.Y., Synek, B.J., Curtis, M.A., Van Roon-Mom, W.M.C., Faull, R.L.M., 2008. The collection and processing of human brain tissue for research. Cell Tissue Bank. 9, 169–179.
Walker, D.G., Lue, L.-F., 2015. Immune phenotypes of microglia in human neurodegenerative disease: challenges to detecting microglial polarization in human brains. Alzheimers Res. Ther. 7, 56.
Wang, J., Milner, R., 2006. Fibronectin promotes brain capillary endothelial cell survival and proliferation through α5β1 and αvβ3 integrins via MAP kinase signalling. J. Neurochem. 96, 148–159.
Wang, G.P., Khatoon, S., Iqbal, K., Grundke-Iqbal, I., 1991. Brain ubiquitin is markedly elevated in Alzheimer disease. Brain Res. 566, 146–151.
Wang, H.-Y., D'andrea, M.R., Nagele, R.G., 2002. Cerebellar diffuse amyloid plaques are derived from dendritic Aβ42 accumulations in Purkinje cells. Neurobiol. Aging 23, 213–223.
Wegiel, J., Wisniewski, H.M., Dziewiatkowski, J., Badmajew, E., Tarnawski, M., Reisberg, B., Mlodzik, B., De Leon, M.J., Miller, D.C., 1999. Cerebellar atrophy in Alzheimer's disease—clinicopathological correlations. Brain Res. 818, 41–50.
Whitney, E.R., Kemper, T.L., Rosene, D.L., Bauman, M.L., Blatt, G.J., 2008. Calbindin-D28k is a more reliable marker of human Purkinje cells than standard Nissl stains: a stereological experiment. J. Neurosci. Methods 168, 42–47.
Xu, J., Patassini, S., Rustogi, N., Riba-Garcia, I., Hale, B.D., Phillips, A.M., Waldvogel, H., Haines, R., Bradbury, P., Stevens, A., 2018. Regional protein expression in human Alzheimer's brain correlates with disease severity. bioRxiv 283705.
Xue, S., Cai, X., Li, W., Zhang, Z., Dong, W., Hui, G., 2012. Elevated plasma endothelial microparticles in Alzheimer's disease. Dement. Geriatr. Cogn. Disord. 34, 174–180.
Xue, Z.-Q., He, Z.-W., Yu, J.-J., Cai, Y., Qiu, W.-Y., Pan, A., Gai, W.-P., Cai, H., Luo, X.-G., Ma, C., 2015. Non-neuronal and neuronal BACE1 elevation in association with angiopathic and leptomeningeal β-amyloid deposition in the human brain. BMC Neurol. 15, 71.
Yamamoto, T., Hirano, A., 1985. Hirano bodies in the perikaryon of the Purkinje cell in a case of Alzheimer's disease. Acta Neuropathol. 67, 167–169.
Zhou, W., Ke, S.Q., Huang, Z., Flavahan, W., Fang, X., Paul, J., Wu, L., Sloan, A.E., Mclendon, R.E., Li, X., 2015. Periostin secreted by glioblastoma stem cells recruits M2 tumor-associated macrophages and promotes malignant growth. Nat. Cell Biol. 17, 170.
Zlokovic, B.V., 2011. Neurovascular pathways to neurodegeneration in Alzheimer's disease and other disorders. Nat. Rev. Neurosci. 12, 723.